Construction and Building Materials 256 (2020) 119390

Contents lists available at ScienceDirect

Construction and Building Materials

journal homepage: www.elsevier.com/locate/conbuildmat

Geopolymer concrete incorporating agro-industrial wastes: Effects on mechanical properties, microstructural behaviour and mineralogical phases

Solomon Oyebisi [a,*], Anthony Ede [a], Festus Olutoge [b], David Omole [a]

[a] Department of Civil Engineering, Covenant University, P.M.B. 1023, Ota, Nigeria
[b] Department of Civil and Environmental Engineering, University of the West Indies, St Augustine, Trinidad and Tobago

HIGHLIGHTS

- Application of both GGBFS and CCA in the production of GPC in ambient curing conditions is attainable.
- CCA replacement level (up to 40%) exhibited higher mechanical strength than PCC.
- The intensity of calcium counts in the SEM-EDX micrographs increased with increasing GGBFS content in the mixture.
- The intensity of silicon counts in the SEM-EDX micrographs increased with increasing CCA content in the mixture.
- C-A-S-H gels are responsible for higher strengths of GGBFS-CCA based GPC.

ARTICLE INFO

Article history:
Received 18 December 2019
Received in revised form 25 April 2020
Accepted 28 April 2020
Available online 8 May 2020

Keywords:
Natural pozzolan
Supplementary cementitious material
Concrete
Microstructure
Compressive strength
Flexural strength
Splitting tensile strength
Alkaline liquid
Waste management

ABSTRACT

The increasing effects of environmental degradation and global warming owing to the production of Portland cement for uses in the construction industry premise the need for sustainable construction materials. This study, therefore, harnessed corncob ash (CCA) and ground granulated blast furnace slag (GGBFS) for the production of geopolymer concrete (GPC) at ambient curing conditions. Corncob was dehydroxylated at 600 °C and partially used as replacement for GGBFS at 0%, 20%, 40%, 60%, 80%, and 100%. The activators used were sodium silicate (SS) and sodium hydroxide (SH), while the molar concentrations of SH were varied at 12 M, 14 M, and 16 M. Moreover, mechanical properties, microstructural behaviour and mineralogical phases of the selected samples were examined. The results revealed that up to 40% CCA replacement level exhibited higher strengths than Portland cement concrete (PCC). Besides, a good relationship exists between the experimental results and the proposed model equations. These proposed models can be beneficial in the development of the strength design of GPC and PCC incorporating agro-industrial wastes. Furthermore, the study shows the possibility of incorporating CCA with GGBFS for production of GPC and the tenability of curing GPC at ambient conditions for the structural application was also attained.

1. Introduction

Concrete is the most universally used material in the construction sector apart from water due to its durability and versatility [1]. Owing to its effectiveness and performance, no other construction materials could compete with concrete when it comes to binding purposes. However, the production of Portland cement concrete (PCC) releases a huge amount of CO_2 into the atmosphere. The global impact of Portland cement (PC)'s production to the earth's surface was estimated to be 7% of the total greenhouse gas emissions (GHG) [2]. The major sources of GHG are the emissions from cement production and other processes from the industrial sector [3–6]. Furthermore, it was established that cement production, fossil fuel combustion, and other industrial processes accounted for 36.2 $GtCO_2$ in 2015 with Nigeria for example, emitting 0.026 $GtCO_2$ in 1970 and 0.870 $GtCO_2$ in 2015. This signifies that the production of PLC has a remarkable influence on the GHG [2]. Developing countries account for CO_2 production with 2.5% yearly increment owing to urbanization [7,8], while 5% yearly increment is attributed to the world cement production [9,10]. Moreover, the negative impacts of this GHG are global warming and environmental dam-

* Corresponding author.
E-mail address: solomon.oyebisi@covenantuniversity.edu.ng (S. Oyebisi).

https://doi.org/10.1016/j.conbuildmat.2020.119390
0950-0618/

age [4,11]. These impacts are contrary to the agenda of the Sustainable Development Goals [12,13]: *"good health and wellbeing"*. In the same vein, Jim et al. [14], Mehta and Burrows [15] and Subramanian [16] stated that deterioration occurs within 10 to 20 years to several concrete structures built in the 20th to the 21st century with PC.

The most potential solution to the growing challenges of GHG and high rate of deterioration of the PCC structures is the adoption of geopolymer concrete (GPC) [17,18]. Supplementary cementitious materials (SCMs), such as fly ash (FA), ground granulated blast furnace slag (GGBFS), metakaolin (MK), rice husk ash (RHA) and silica fume (SF) are utilized as binders for the production of GPC [17,19,20]. These materials consist mostly, calcium silicates and aluminosilicates, and are activated with SS and SH solutions to produce a geopolymer binder [17–19]. A lot of greener interest has been generated for GPC in the field of chemistry and engineering ever since its introduction by Davidovits in 1978. Apart from its environmental friendliness, GPC has become one of the possible alternatives to PCC due to its excellent durability properties [17,18], lower heat of hydration and excellent resistance against sulfate and acid [1,18,21], higher mechanical strength [22–24], and economic advantage [25,26]. In the construction industry, geopolymer concrete emerged as a greener concrete technology as a result of the global call for sustainable building and environment. The GPC, unlike PC, depends on natural materials or industrial by-products with the minimized process to provide the binding agent. Davidovits [8] stated that the total energy required to produce a geopolymer cement slag by-product is 1965 MJ/tonne, while that of PLC is 4700 MJ/tonne, thus indicating a decrease of 59% in the geopolymer cement compared with PLC. Therefore, the use of agro-industrial wastes, such as FA, GGBFS, CCA, MK, SF and RHA, have been used to partially or fully replace PLC for production of GPC and solid blocks and the results were suitable. It was reported by Oyebisi et al. [26] that the global production of corn was 969.69 and 1071.51 million metric tons in 2016 and 2017, respectively. However, most of the corncobs produced are disposed as waste, hence culminating in environmental pollution. This justified the selection of CCA in the production of GPC. Furthermore, CCA has been used as a pozzolanic material to partially replace PC for the production of concrete and mortar [27] and solid blocks [28,29] to improve their workability [30,31], durability [32] and thermal insulating properties [33,34]. However, no study has been carried out to examine the effects of CCA blend on the mechanical, microstructural, and mineralogical properties of slag-based GPC. Besides, CCA exhibits both pozzolanic and cementitious properties in that CaO content $\geq$10% and $\leq$20% [32]; and the silica content is highly reactive, thus enhancing the potential of the aluminosilicate gel, which provides mechanical strengths to the GPC [8]. On the other hand, type, mineralogical, and chemical compositions of aggregates also play a vital role and influence on the concrete performance, apart from the agro-industrial by-products used for its production [35,36].

Many studies in the literature reported favourable performance of GPC under ambient curing conditions. Deb et al. [37] investigated the properties of GGBFS-FA based GPC cured at ambient temperature (15 to 20 °C). A constant ratio of SS to SH was selected as 2.5. The results indicated an increase in compressive strength with age. The early strength was also improved with increasing GGBFS content in the mixture. In addition, good workability and higher strength were observed with increasing GGBFS content up to 20% compared with PCC, meanwhile, the drying shrinkage of GPC decreased as the GGBFS content increased from 1% to 20%. Moreover, Irani et al. [38] examined the properties of FA based GPC incorporating GGBFS at 20%, 40%, 50%, 60% and 80% of FA. The ratios of SS to SH were varied from 1:5 to 2.5 at various molarities of SH as 8 M, 10 M and 12 M using a different alkaline liquid to binder (Al/B) ratios of 0.45, 0.50 and 0.55. It was revealed that the addition of GGBFS improved the polymerization of the GPC mix at ambient temperature, resulting in good compressive strength. A marginal increase was also noticed in compressive strength as the molarity of SH increased from 8 M to 12 M. The mix proportion of 40% FA and 60% GGBFS and the Al/B ratio of 0.5 exhibited the highest compressive strength compared with other mix proportions and Al/B ratios. Furthermore, Hadi et al. [39] designed and cured a GPC incorporating GGBFS, FA, MK and SF at room temperature using the Taguchi method. The highest compressive strength was discovered at 7 days with mix proportion, consisting Al/B ratio of 0.35, and SS/SH ratio of 2.5 at 14 M. In addition, the setting times of the geopolymer pastes were enhanced and the slump increased as GGBFS was partially replaced with FA, MK, and SF. However, the compressive strength of GGBFS- based GPC was reduced with increasing FA, MK, and SF content in the mixture. Lee and Lee [40] also investigated the properties of FA-GGBFS based GPC cured and produced at ambient conditions. The results indicated a decrease in setting time with increasing GGBFS content and SH concentration in the mix. Similarly, Nath and Sarker [41] studied the properties of GGBFS-FA based GPC cured at ambient conditions (20 to 23 °C). The experimental results revealed a decrease in the set times and workability of GPC with increasing GGBFS content in the geopolymer mixture. At 28 days, it was also revealed that for each 10% increase in the GGBFS content, the strength under compression increased by 10 MPa. Oyebisi et al. [22] examined the effects of alkali concentrations on the mechanical properties of GGBFS-CCA based GPC in ambient curing conditions at a 2.5 constant ratio of SS to SH. A grade 30 MPa concrete was used as mix proportion and tested at 7 and 28 days. The results showed the highest compressive strength of 40% CCA and 60% GGBFS replacement level at 14 M of SH solution compared with 12 M and 16 M.

There is no study on the long-term mechanical strengths, microstructures and strength prediction of CCA-GGBFS based GPC cured in ambient conditions. Thus, the overall aim of this study is to investigate the effect of replacing GGBFS with CCA on the mechanical strengths of GPC at 7, 28, 56 and 90 days in ambient conditions. The microstructure and mineralogical phase of the selected samples were analyzed using Scanning Electron Microscopy equipped with Energy Dispersive X-ray (SEM-EDX) and X-ray Diffraction (XRD), respectively, to characterize how each species and mineralogical phases contributed to the mechanical performance of the geopolymer mixture. Finally, model equations were developed to correlate the mechanical strengths of GPC incorporating agro-industrial wastes.

2. Experimental programme

2.1. Materials

GGBFS, CCA, alkaline liquid (Al), and aggregates were majorly used in this study. Portland limestone cement (PLC) was used as a binder for the production of PCC and compared it with GPC. Slag was sourced from the Federated Steel Mills Limited, Ota, Nigeria (60 40′ 04. 84″ N; 30 11′ 43.85″ E). The material was ground to obtain GGBFS and sieved with BS 90 μm sieve to reflect the properties of cement as shown in Fig. 1. The specific gravity and fineness of the GGBFS are 3.10% and 7.6%, respectively. Corncobs was soured from Agbonle (8° 53′ 13.49″N; 3° 31′ 12.46″ E). It was dehydroxylated at 600 °C to obtain CCA as shown in Fig. 1. The specific gravity and fineness of the CCA are 2.44% and 8.0%, respectively. PLC grade 42.5R, classified as CEM II class of cement as defined by both Nigerian Industrial Standard (NIS) [42] and BS EN 197-1 [43], was used as shown in Fig. 1 to fulfil the requirements recommended by NIS 441-1 [44] and approved by the Standards Organi-

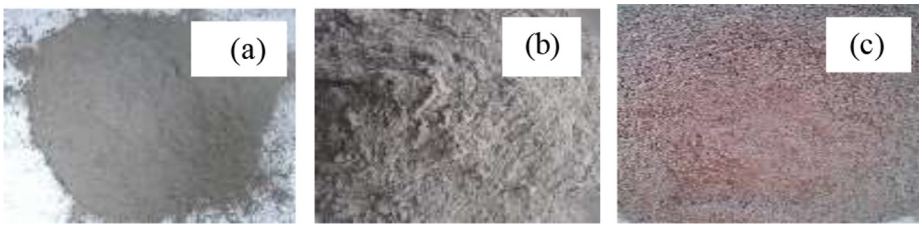

Fig. 1. Binders (a) PLC (b) GGBFS (c) CCA.

zation of Nigeria [45]. The specific gravity and fineness of the PLC are 3.15% and 7.5%, respectively. The specific gravity was determined in consonance with the requirements stated by BS EN 196-3 [46] using a specific gravity bottle and kerosene. In the same vein, the fineness of all the binders was determined in accordance with the specifications stipulated by BS EN 196-6 [47] using the dry sieving method and BS sieve 90 μm. From the results obtained, the specific gravity of PLC met the 3.15 maximum requirement of BS EN 193-3 [46], and thus, suitable for use. Similarly, the specific gravity of GGBFS fulfilled the 3.10% to 3.15% requirement of BS EN 15167-1 [48]. Meanwhile, the specific gravity of CCA was similar to the results obtained by Oyebisi et al. [22,23]. Moreover, the fineness test results obtained for GGBFS, CCA and PLC met the 12% maximum specification of BS EN 196-6 [47,49,50]; hence desirable for use as binders. Furthermore, the oxide compositions of GGBFS, CCA and PLC were examined using the XRF spectrophotometer machine, Philips PW-1800.

Fine aggregate (FAgg) and coarse aggregate (CAgg) were sourced locally. Prior to developing mix designs, the materials were prepared at the saturated dry surface, and grading was conducted to affirm and obtain the required particle size distribution. In addition, tests were performed to characterize the aggregates based on BS EN 12620 [51]. The specific gravity of aggregates was determined in consonance with BS EN 12620 [51]. The test results showed a specific gravity of 2.60% and 2.64% for FAgg and CAgg, respectively. In the same vein, the water absorption was determined in accordance with the procedure earlier stated for the specific gravity. The results indicated a water absorption of 0.7% and 0.8% for FAgg and CAgg, respectively. On the other hand, the moisture content for both fine and coarse aggregates was obtained in accordance with BS EN 12620 [51] using a clean container with its lid. The results signified a moisture content of 0.3% and 0.2% for FAgg and CAgg, respectively. The particle size distributions of the aggregates are shown in Fig. 2, indicating that both aggregates met the limits of BS EN 12620 [51], hence suitable for use. Furthermore, the mineralogical composition of the coarse aggregate (granite) was identified with the aid of Petrological Microscope. The sample was prepared, polished in glass ground plate using carborundum, and mounted on a clean glass slide with adhesive [35]. On the other hand, the chemical composition of the coarse aggregate was analyzed with the aid of the XRF spectrometer machine, Philips PW-1800. The results of mineralogical composition showed Quartz, Feldspar, Mica, and Iron oxide as 62.50%, 20.45%, 16.55%, and 0.50%, respectively. Moreover, the chemical composition of the coarse aggregate revealed SiO_2, Al_2O_3, Fe_2O_3, CaO, MgO, SO_3, K_2O, Na_2O, P_2O_5, MnO, and LOI as 67.05%, 14.40%, 5.63%, 3.90%, 1.72%, 0.02%, 5.50%, 1.16%, 0.15%, 0.05%, and 0.52%, respectively. From these results, it can be inferred that the coarse aggregate is acidic granite owing to the fact that the content of SiO_2 was in the range of 66% to 75% [52,53]. In addition, on the basis of alkalinity, the granite was classified as calcalkalinity in that $(Na_2O + K_2O)^2/(SiO_2 - 43)$ was 1.85 which ranged between 1.2 and 3.5 for calcalkalinity [36].

The alkaline liquids used in this study were SH pellets comprising 99% purity, and SS gel sourced from a chemical dealer in Lagos, Nigeria. These alkaline liquids were adopted because they buffer the pH of the geopolymer pastes and increase the mechanical properties of the final product [9,17–20,22]. The SH pellets of 354 g, 400 g, and 443 g were measured and dissolved in 646 g, 600 g, and 557 g of clean water for the 12 M, 14 M, and 16 M, respectively, based on the chemistry standard laboratory procedures established by Rajamane and Jeyalakshmi [52], and as previously used for production of GPC [22]. Prior to casting, the solutions were prepared 24 h earlier, to reduce the high rise in temperature as a result of the reaction between SH pellets and water. After 2 h, the SH solution was added to SS gel for better performance [22,41] at a constant ratio of SS/SH as 2.5:1. The water used for mixing was clean and conformed to BS EN 1008 [53].

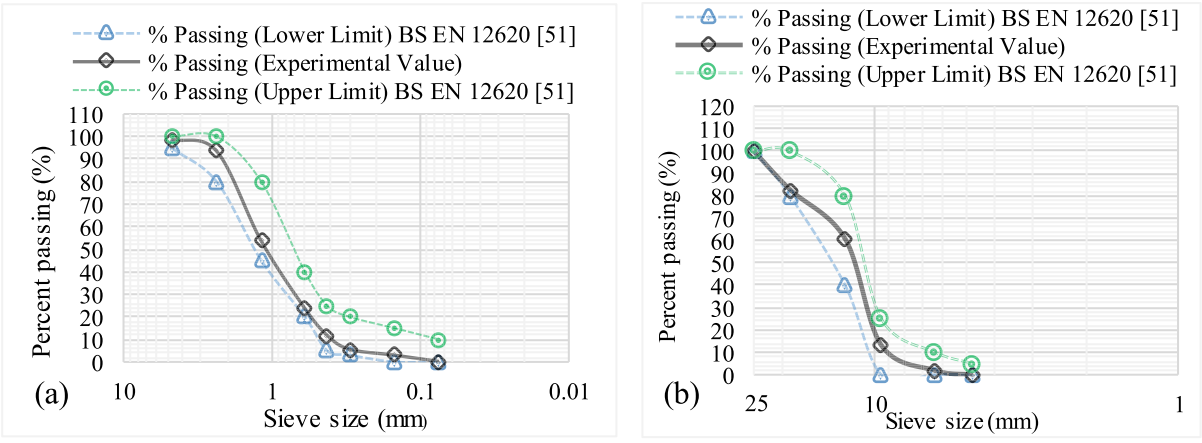

Fig. 2. Particle size distribution (a) Fine aggregate (b) Coarse aggregate.

2.2. Mix proportions

Geopolymer concrete design has no specific code or standard. In the course of this study, the BS EN 206 [54] was used as a guide to obtaining the initial mix proportions for both M 30 and M 40 target strengths. The batching method of materials by weight was adopted to obtain accurate desired concrete. The percentage substitutions of both GGBFS and CCA were selected based on the applicable findings that the compressive strengths of CCA blended concrete are attainable at 20 to 30% replacement levels for structural applications [22,27,55–57]. But, the substitution of CCA was proportioned at 0%, 20%, 40%, 60%, 80% and 100% of the volume of GGBFS, denoting G1, G2, G3, G4, G5 and G6, respectively, to examine the replacement levels which would meet the target strengths for both structural and non-load bearing applications. The results obtained were compared with the same properties of a control concrete (PCC), containing 100% PLC. Tables 1 and 2 present the concrete mix design proportions (quantities) for both grades 30 MPa (M 30) and 40 MPa (M 40), respectively.

2.3. Mix preparation, casting and curing

Fresh GPC was prepared, mixed, and manually cast in accordance with the requirements stipulated in the BS 1881-125 [58] and BS EN 12390-2 [59] for PCC. The concrete constituents were thoroughly mixed for about 15 min at a temperature of 25 to 28 °C and a relative humidity (RH) 60 ± 5% until a homogenous mixture was obtained. The freshly made concrete was poured into a standard 150 mm cubical mould for compressive strength tests; 300 mm long cylindrical mould for splitting tensile strength tests; and 600 mm long beam for flexural strength tests. The samples were compacted each in three layers with the aid of a 16 mm diameter tamping rod. For each mix ID, a total of 12 samples were made per grade of each strength test. After 48 h, the GPC samples were removed from the mould to allow for better polymerization following the similar study [22], which reported better mechanical performances compared with 24 h removal. The samples were cured under the ambient conditions (25 to 28 °C and 60 ± 5% RH), and tested at 7, 28, 56 and 90 days, while the immersion method of water curing was adopted for the PCC samples.

2.4. Testing procedures

2.4.1. Workability tests

The workability properties, consistency and setting times were carried out in line with the procedure stated in BS EN 196-3 [46], while slump and compacting factor were conducted on the fresh samples following the procedures stipulated in BS EN 12350-2 [60] and BS EN 12350-4 [61], respectively.

2.4.2. Mechanical tests

The mechanical strength tests were carried out with the aid of an INSTRON 5000R UTM in a constant force regime under a loading rate of 0.6 MPa per second for the compressive strength tests; 0.06 MPa per second for the flexural strength tests; and 0.04 MPa per second for the splitting tensile strength tests in consonance with BS EN 12390-4 [62]; BS EN 12390-5 [63]; and BS EN 12390-6 [64], respectively. Experimental tests were conducted on three samples per testing day for each mix ID. The average values were calculated and obtained, and the results were used.

2.4.3. Microstructural analysis

SEM-EDX, Model JEOL 70006000 was used to characterize the microstructure and the chemical compositions of the concrete samples at 28-day of hydration. The EDX analysis was performed on a flat (general) scan. For the analysis, the working distance was ranged between 8.2 and 10.6 mm while the accelerated voltage was constant at 15 kV on the concrete samples, PCC, G1, G2, G3, G4, G5 and G6 for M 40. The prepared samples were firmly placed in an aluminium holder stub with the aid of double sticky carbon tape, and carbon-coated. Besides, the morphology was performed on the selected concrete samples with the aid of SEM analysis in the secondary electron mode at 7 and 28 days of curing. The selected concrete samples (PCC, G1, and G6) for M 40 were observed at 60 to 100x magnification in a high vacuum to examine the compatibility and cohesiveness of the modified mix.

2.4.4. XRD analysis

The mineralogical phases and connectivity pattern of the silicon and aluminium species present in the selected samples, PCC, G1, and G6 for M 40 were investigated. After 28 days hydration, the samples were prepared as finely ground powder to reveal the accurate information on the phase identification and chemical composition of the sample, and acquired by a scanning rate of 1^0 per min from 0 to 60^0 at a scanning angle (2θ) using XRD instrument, Model ADX-2500, with a generated radiation of Cu-kα in 40 mA and 45 kV at room temperature.

2.4.5. Prediction of mechanical strengths

This study proposed model equations using the general model power in Matlab R2017a. The proposed model equations were compared with both the experimental data and the model equations developed from previous studies (as shown in Table 3) to validate the accuracy and applicability of the models.

3. Result and discussions

3.1. Oxide compositions of binders

In Table 4, CCA fulfilled the conditions recommended by BS EN 450-1 [72] and BS EN 8615-2 [73] such that the addition of SiO_2, Al_2O_3, and Fe_2O_3 met the minimum requirement of 70%. In addition, the LOI of less than 10% was also fulfilled [72,73]. The maximum requirements of 3%, 4%, and 5% for the contents of SO_3, MgO, and Na_2O were also fulfilled respectively [72,73]. Furthermore, the CaO content ranging between 10 and 20% recommended

Table 1
Mix proportions for M 30 (in Kg/m^3).

Mix ID	PLC	GGBFS	CCA	FAgg	CAgg	SH	SS	SS/SH	Al/B
PCC	390	0	0	675	1031	0	0	0	0.54
G1	0	390	0	675	1031	60	150	2.5	0.54
G2	0	312	78	675	1031	60	150	2.5	0.54
G3	0	234	156	675	1031	60	150	2.5	0.54
G4	0	156	234	675	1031	60	150	2.5	0.54
G5	0	78	312	675	1031	60	150	2.5	0.54
G6	0	0	390	675	1031	60	150	2.5	0.54

Al/B is the alkaline liquid-to-binder ratio.

Table 2
Mix proportions for M 40 (in Kg/m^3).

Mix ID	PLC	GGBFS	CCA	FAgg	CAgg	SH	SS	SS/SH	Al/B
PCC	500	0	0	585	1031	0	0	0	0.42
G1	0	500	0	585	1031	60	150	2.5	0.42
G2	0	400	100	585	1031	60	150	2.5	0.42
G3	0	300	200	585	1031	60	150	2.5	0.42
G4	0	200	300	585	1031	60	150	2.5	0.42
G5	0	100	400	585	1031	60	150	2.5	0.42
G6	0	0	500	585	1031	60	150	2.5	0.42

Table 3
Model equations developed from previous studies

S/N	Model			
	Development	Proposed type	Validating equation	Author
1	Splitting tensile strength (f_{ct}) and compressive strength (f_c)	Power	$f_{ct} = 0.36fc^{0.50}$	AS 3600 [65]
			$f_{ct} = 0.67fc^{0.50}$	Neupane [66]
			$f_{ct} = 0.30fc^{0.67}$	BS EN 1992-1:1 [67]
			$f_{ct} = 0.50fc^{0.50}$	Sofi et al. [68]
			$f_{ct} = 0.616fc^{0.50}$	Tempest [69]
			$f_{ct} = 0.249fc^{0.772}$	Lavanya and Jegan [70]
2	Flexural strength (f_r) and compressive strength (f_c)	Power	$f_r = 0.60fc^{0.50}$	AS 3600 [65]
			$f_r = 0.88fc^{0.50}$	Neupane [66]
			$f_r = 0.40fc^{0.70}$	BS EN 1992-1:1 [67]
			$f_r = 0.60fc^{0.50}$	Sofi et al. [68]
			$f_r = 0.69fc^{0.50}$	Diaz-Loya et al. [71]

Table 4
Oxide compositions of binders used.

Oxide composition	CaO (%)	SiO_2 (%)	Al_2O_3 (%)	Fe_2O_3 (%)	MgO (%)	SO_3 (%)	K_2O (%)	Na_2O (%)	P_2O_5 (%)	MnO (%)	TiO_2 (%)	LOI (%)
CCA	12.62	60.50	8.78	9.13	1.23	1.25	1.25	0.65	0.20	1.20	1.35	2.89
GGBFS	36.52	35.77	14.11	0.92	9.45	1.08	0.52	0.30	0.09	0.65	0.70	1.32
PLC	64.90	21.60	5.85	2.78	1.42	2.03	0.72	0.14	–	–	–	1.38

Loss of Ignition (LOI) at 800 °C.

by Al-Akhras [74] for the pozzolanic and cementitious materials were met. Above all, the oxide content of CCA used in this study affirmed the similar content obtained in the previous studies [22,23,30,75–77]. Therefore, the conclusion that CCA could exhibit pozzolanic reactivity can be inferred because amongst other requirements being fulfilled, silica content of 25% minimum was also met [73]. On the other hand, both silica (SiO_2) and lime (CaO) contents of GGBFS met the BS EN 15167-1 [48]'s limit requirements of 32 to 40%. The LOI's requirement of 0.5 to 3.0% for GGBFS stated by BS EN 15167-1 [48] was also met. The chemical moduli of $(CaO + MgO/SiO_2) \geq 1$, $(CaO/SiO_2) \leq 1.4$, and $SiO_2 + CaO + MgO \geq 67\%$ for cementitious materials recommended by BS EN 15167-1 [48] were fulfilled. Therefore, it can be asserted that GGBFS exhibited both pozzolanic and cementitious/hydraulic reactivity [74,78,79]. Moreover, the oxide contents of GGBFS used in this study exhibited similar contents obtained from previous studies [22,23,37–40,78]. Finally, the PLC satisfied the chemical requirements of BS EN 196-2 [80].

3.2. Workability properties

3.2.1. Consistency and setting time

Fig. 3 illustrates the consistency, initial setting times (Ist), and final setting times (Fst) of the fresh samples prepared with 12 M, 14 M, and 16 M activators. It was revealed, as shown in Fig. 3(a), that the consistency increased with increasing CCA content in all levels of activators. Besides, as the percentage replacement of CCA increased in the blended mix, both initial and final setting

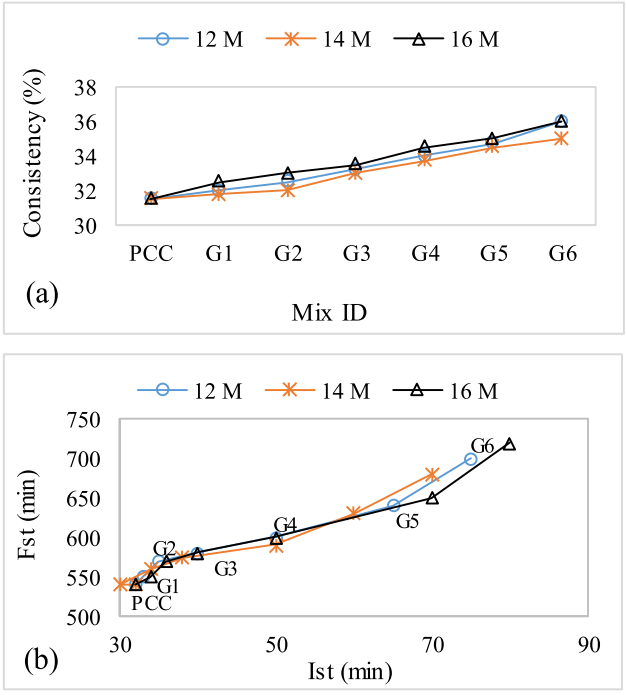

Fig. 3. Fresh samples properties (a) consistency and (b) setting times.

times increased at all levels of activators, as shown in Fig. 3(b). The reason for an increase in consistency and setting times could be attributed to the reduction in interfacial particle of GGBFS with increasing CCA content. Thus, more water is needed to form paste of same consistency for various substitution of CCA in the blended mix, hence increasing consistency and setting times. Also, as the CCA content in the mix increases, the intensity of G6 were 15% and 20% higher than Fst recommendation [46], and can be applied in hot weather condition. CaO counts in GGBFS reduces. This delays the polymerization process, thus causing an increase in setting times. Kamau et al. [27] and Adesanya and Raheem [75,76] also reported the similar findings that CCA caused an increase in setting times when blended with PC for concrete production. To this end, G1, G2, G3, and G4 yielded the similar results with control paste (PCC) and satisfied a minimum of 45 min for Ist and 600 min for Fst, recommended by of BS EN 196-3 [46]. Therefore, mixes G1, G2, G3, and G4 can be applied in normal weather condition. In contrast, G5 and G6 were 15% and 20% higher than Fst recommendation [46], and can be applied in hot weather condition.

3.2.2. Slump and compacting factor

Fig. 4 (a) and (b) present the slump and compacting factor (Cf) results of the fresh concrete samples for M 30 and M 40, respectively. It was revealed that slump increased with compacting factor. Also, an increase in CCA content in the blended mix led to an increase in slump and compacting factor of the fresh concrete samples at all levels of activators for both M 30 and M 40. The reason may be ascribed to the internal voids and specific surface area of CCA particles being higher than GGBFS particles; this slows the rate of setting times, hence increasing the slump value. Moreover, the interfacial particle of GGBFS was reduced due to the lower specific gravity of CCA compared with GGBFS. Consequently, it increases the setting times, thus increasing the slump. In a related study, Nath and Sarker [41] reported that the slump value of GGBFS-based GPC increases with increasing fly ash content (pozzolan). Besides, Adesanya and Raheem [75,76] established that CCA increases the setting time of concrete paste, hence increasing the slump value. Pozzolanic material is known for low rate of heat development and it is of great advantage in mass concrete, because it reduces the thermal stress [75]. Moreover, unlike 12 M and 16 M activators, 14 M activator exhibited a reduction in slump and compacting factor values at all levels of CCA replacement for both M 30 and M 40. This could be attributed to the greater capacity of 14 M to dissolve and liberate aluminosilicate monomers in the blended mix than 12 M and 16 M, hence accelerating the polymerization process and causing better performance. However, at 16 M activator, OH– solution could be excessive in the mix, which limits the mobility and potential to interact with reactive species, hence increasing the slump and delaying polymerization process [18]. Ultimately, the results obtained therein can be applied in normal reinforced concrete work without vibration and heavily reinforced sections with vibration, because they met 50 to 150 mm for slump and 0.700 to 0.950 for compacting factor, as recommended by BS EN 12350-2 [60] and BS

EN 12350-4 [61], respectively.

3.3. Mechanical strengths

3.3.1. Compressive strength (CS)

The results of CS for both M 30 and M 40 are presented in Fig. 5 following the procedure stipulated in BS EN 12390-4 [60]. The results revealed that the compressive strength of the GPC increased as the GGBFS replacement level in the mix increased. This could be attributed to the aluminosilicate glassy phase of GGBFS, which dissolves when reacts with alkaline activators, and results in x-ray amorphous aluminosilicate gel, thus responsible for better mechanical performances of the hardened concrete. It also suggests that GGBFS is a better aluminosilicate material [1,19,20]. Besides, the increase in strength may be attributed the workability of GPC in that the workability properties, setting times, slump, and compacting factor of GPC incorporating both GGBFS and CCA reduced with increasing GGBFS content owing to the higher specific gravity of GGBFS compared with CCA, and which consequently increased the calcium counts in the geopolymer pastes, reduced the rate of workability, and increased the strength performance of GPC. However, below 60% replacement level of GGBFS by CCA in the mix, the compressive strength decreased when compared with that of the PCC. This signifies that GGBFS-CCA-GPC attains its optimum compressive strength at 60% GGBFS and 40% CCA when compared with the strength of PCC of the same grade. This reduction in compressive strength of GGBFS-CCA-GPC above 40% CCA replacement level may be attributed to the insufficient CaO in pozzolanic material (CCA) to combine with aluminosilicate material (GGBFS) to form Calcium aluminate silicate hydrate (C-A-S-H) which gives the strength to GPC [20]. Comparing the three activators, the results indicated that 14 M activator exhibited the highest compressive strengths with 48.23 MPa and 59.76 MPa at 90 days curing when compared with 40.05 MPa and 51.12 MPa for PCC for M 30 and M 40, respectively. This is agreeable with Hadi et al. [39] that a GPC incorporating GGBFS as the aluminosilicate source exhibits optimum CS at 14 M activator of the SH concentration. Statistically, a percentage increase in GPC's strength by 22.93%, 17.96% and 8.54% was observed for G1, G2 and G3, respectively, compared with PCC's strength at 28 days of curing for M 30. Meanwhile, in comparison with PCC's strength at 28 days for 14 M activator of M 40, a percentage increase in GPC's strength by 15.60%, 11.41% and 5.26% for G1, G2 and G3 respectively was established. In the same vein, at 12 M activator, GPC signified a percentage increase in strength by 18.65%, 12.48% and 6.17% for G1, G2, and G3, respectively, compared with PCC's

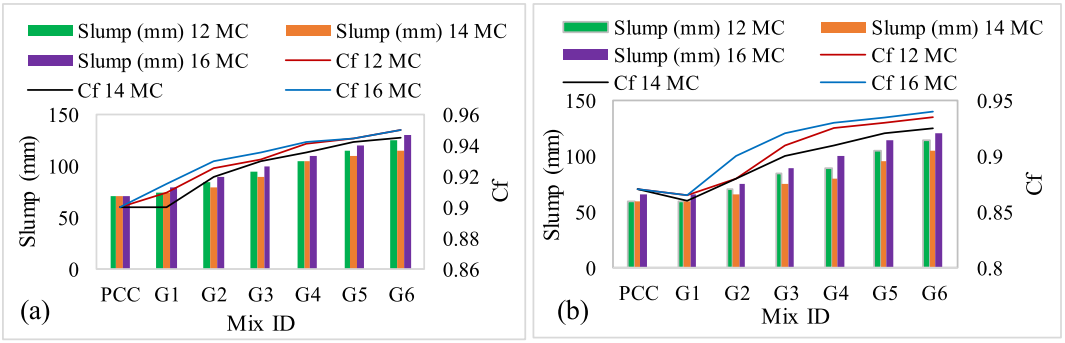

Fig. 4. Slump and compacting factor for (a) M 30 and (b) M 40.

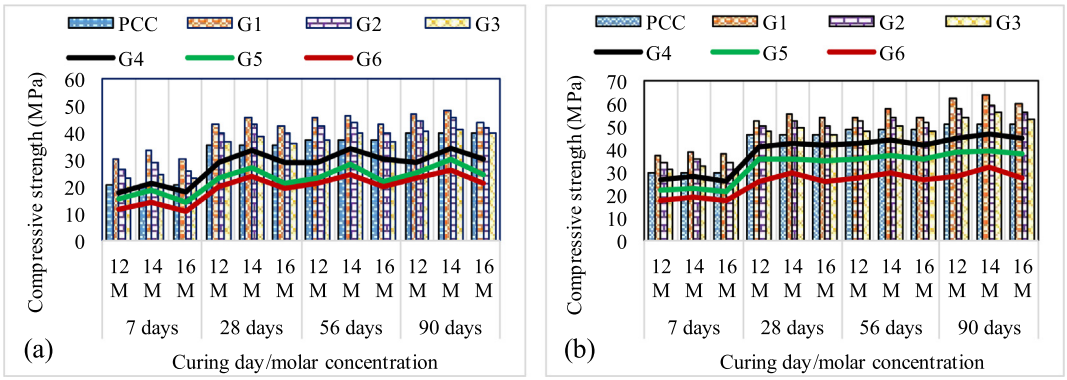

Fig. 5. Compressive strength (a) M 30 (b) M 40.

strength at 28 days of curing for M 30. Also, in comparison with PCC's strength at 28 days for M 40, a percentage increase in GPC's strength by 11.29%, 7.41% and 2.22% were respectively obtained for G1, G2 and G3 for 12 M activator. On the other hand, at 16 M activator, a percentage increase in GPC's strength by 17.35%, 12.09% and 2.74% % were respectively observed for G1, G2 and G3 compared with PCC's strength at 28 days for M 30. Likewise, a percentage increase in GPC's strength by 10.97%, 6.79% and 0.10% were respectively obtained for G1, G2 and G3 for 16 M activator, compared with PCC's strength at 28 days for M 40. The results affirmed the previous studies on GGBF-FA based GPC such that GPC's strength increased with increasing in GGBFS content and marginally increased with increasing age [37,39,41]. Therefore, in comparison with PCC, an improved strength of G1, G2 and G3 both in early and later ages can be ascribed to the reactive presence of calcium-silicate-aluminate-hydrate (C-S-A-H) in the geopolymer paste which compacted the microstructure and reduced the pores of geopolymer matrix, hence accelerating the mechanical strengths of the GPC [41,49,78,81].

The results of CS for 16 M activator were marginally decreased compared with 12 M and 14 M activators for both grades of concrete. This signified that the compressive strength increased as the molar concentration of SH solution increased from 12 to 14 M activator but decreased at 16 M activator. Meanwhile, the effect of SH concentration on the compressive strength of the GPC has not been totally agreed upon by the researchers. Some of the studies in the literature reported an increase in compressive strength owing to the high concentration of SH solution in the GPC mixture [9,19,20,82] such that more aluminosilicate will be dissolved, and consequently, speeds up the polymerization reaction and boosts the mechanical strength of GPC [83]. However, some other studies revealed a decrease in compressive strength due to more concentration of SH solution in the GPC mixture [84]. The results obtained from this study supported the previous study on GGBFS-FA based GPC activated with 8–16 M activator and cured at ambient conditions [38]. It reported an increase in compressive strength as the molar concentration of SH solution increased from 8 to 14 M activator at the percentage replacement level of 40% FA and 60% GGBFS but at 16 M activator, the strength decreased. Owing to these results and the previous studies, the reduction in compressive strength of GGBFS-CCA based GPC at 16 M activator for all replacement levels may be attributed to the development of hygroscopic due to the reaction of excess alkali with atmospheric CO_2 to form sodium carbonate crystals, resulting in the cosmetic product rather than binding product [85]. Furthermore, the amorphous structure of the source materials (GGBFS and CCA) could be encased in the spheres and caused the deposit of alkali reaction products to act as a barrier to alkaline dissolution. Therefore, it is inferred that the optimum replacement level of agro-industrial wastes for production of GPC to meet the target strength as well as surpass the strength of PCC (control) is 60% GGBFS and 40% CCA for both grades of concrete, and at all levels of molar concentrations of SH solutions but 14 M activator is suitably preferable. This result can be used for structural application as it structurally fulfilled the required limits specified by BS EN 1992:1-1 [67] and BS EN 8500-1 [86] for a structurally designed concrete structure.

3.3.2. Flexural strength (FS)

The results of flexural strength for both M 30 and M 40 following the procedure highlighted in BS EN 12390-5 [63] are presented in Fig. 6. The results exhibited a similar trend with the results of compressive strength at all replacement levels and molar concentrations of SH solutions, indicating that both compressive and flexural strengths exhibited a good level of agreement. The results also indicated that the flexural strength increased with increasing compressive strength in all types of concretes produced. This confirmed Neville [49] that flexural strength increases with increasing compressive strength. Moreover, the GPC activated with 14 M activator produced the maximum flexural strength compared with that of 12 M and 16 M activators.

The analysis of percentage increase in Fig. 6 (a) for M 30 revealed that 14 M of G1, G2 and G3 at 7, 28, 56 and 90 days respectively exhibited higher flexural strength of 32.09%, 16.48%, 13.39% and 17.06%; 31.34%, 18.97%, 13.95% and 14.70%; and 11.19%, 11.49%, 10.46% and 9.80% than the PCC. Similarly, the analysis of percentage increase in Fig. 6 (b) for M 40 indicated that 14 M of G1, G2 and G3 at 7, 28, 56 and 90 days respectively manifested higher flexural strength of 18.11%, 11.40%, 12.70% and 16.35%; 12.96%, 6.30%, 8.04%, and 11.48%; and 8.85%, 4.40%, 2.09%, and 7.55% than the PCC. These results confirmed the findings of Fernandez-Jimenez et al. [18], Neupane [66], and Raijiwala and Patil [87] that GPC possesses around 15% higher flexural strength than the PCC of the same grade. It also affirmed the results of Olivia and Mikraz [88] that flexural strength of FA-based GPC is around 1 to 1.4 times higher than PCC at 28 and 90 days; and 8 to 12% higher flexural strength than PCC at 28 and 90 days. The increase in flexural strength of GPC may be attributed to the effective bonding between the aggregate content and the matrix of geopolymer mixture [19,20,88]. Owing to these results, it can be proved that GGBFS-CCA based GPC resists more bending or stress under applied load than PCC.

3.3.3. Splitting tensile strength

Fig. 7 presents the results of splitting tensile strength for both M 30 and M 40 following the methods outlined in BS EN 12390-6 [64]. The results showed a similar trend with the results of compressive strength at all replacement levels and molar concentra-

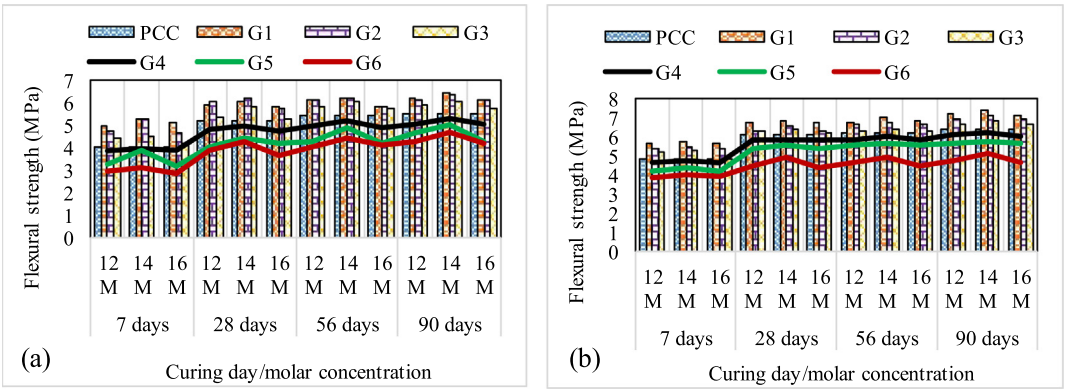

Fig. 6. Flexural strength (a) M 30 (b) M 40.

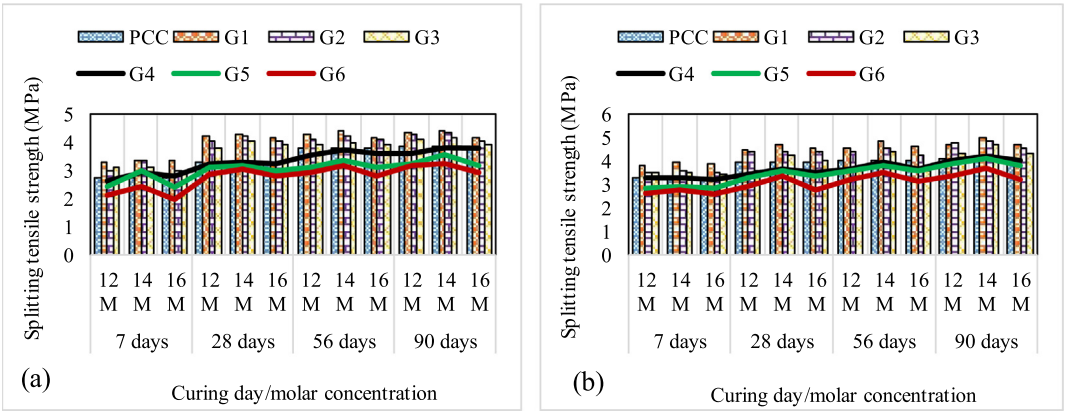

Fig. 7. Splitting tensile strength (a) M 30 (b) M 40.

tions of SH solutions, signifying that both compressive and splitting tensile strengths manifested a good level of agreement. The results showed that the splitting tensile strength increased with increasing compressive strength. This supported Neville [49] that splitting tensile strength increases as the compressive strength increases. Statistically, the percentage increase in Fig. 7 (a) for M 30 showed that 14 M activator of G1, G2, and G3 at 7, 28, 56 and 90 days respectively possessed higher splitting tensile strength of 23.99%, 29.52%, 16.05% and 14.06%; 23.62%, 26.21%, 10.79% and 12.76%; and 15.13%, 20.78%, 4.74% and 8.85% than the PCC. In the same vein, the analysis of the percentage increase in Fig. 7 (b) for M 40 showed that 14 M activator of G1, G2 and G3 possessed 19.51%, 18.69%, 19.65% and 20.39%; 8.23%, 11.11%, 12.19% and 16.75%; and 6.40%, 6.82%, 8.96% and 13.84% higher splitting tensile strength than the PCC at 7, 28, 56 and 90 days, respectively. These results supported the findings of Fernandez-Jimenez et al. [18], Neupane [66], and Raijiwala and Patil [87] that GPC possesses around 15% higher splitting tensile strength than that of PCC of the same grade of concrete. In addition, the results confirmed the findings of Olivia and Mikraz [88] that splitting tensile strength of FA-based GPC is 8 to 12% higher than PCC at 28 and 90 days of curing. Moreover, the results corroborated the findings of Bouaissi et al. [1] who reported a 10 to 11% higher splitting tensile strength for FA-GGBFS based GPC than PCC at 28 and 90 days of curing at ambient conditions. The increase in flexural strength of GPC reflected the effective bonding between the aggregate content and the matrix of geopolymer mixture [19,20,89]. Therefore, it can be established that GGBFS-CCA based GPC resists more splitting tensile under an applied load or induced stress than the PCC.

3.4. Microstructures of GPC and PCC

3.4.1. SEM-EDX analysis

The results of microstructures and elemental compositions of the concrete samples, PCC and G1 to G6 for M 40 at 28-day of hydration are presented in Figs. 8 and 9 using SEM-EDX analyzer. The SEM micrographs observed in PCC, as indicated in Fig. 8 (a), showed the irregular shape with traces of sharp needles. The chemical reaction between the lime content (CaO) present in the PLC powder and the water produced a hydrating agent called "calcium-silicate-hydrate gel (C-S-H)". Moreover, this hydrating agent then mixed with Ca(OH)2 available in the cement pastes as well as quartz in aggregates to produce a hardened network, and thus responsible for the mechanical strengths of PCC [49,83]. Besides, adequate cohesiveness and good interface were evident from the morphological analysis of this sample. Moreover, the SEM micrographs as shown in Fig. 8 (b), (c), (d), (e) and (f) was amorphously structured in spherical flakes with sharp needles. The lime content (CaO) in the GGBFS powder reacted with the alkaline activator to form Ca(OH)2 [49]. The Ca(OH)2 reacted with SiO2 and Al2O3 present in the GGBFS and CCA powders, thus forming calcium-aluminate-silicate-hydrate (C-A-S-H); and this could be responsible for the higher mechanical strength of the G1, G2, and G3 compared with that of PCC [50]. In the same vein, Nath and Sarker [41] and Yang et al. [90] stated that the formation of C-A-S-H gel in GGBFS-FA based GPC was as a result of an increase in calcium counts with increasing GGBFS content in the mixture, thus resulting in higher mechanical strengths compared with that of PCC. Also, a better interface was noticed for this sample based on its

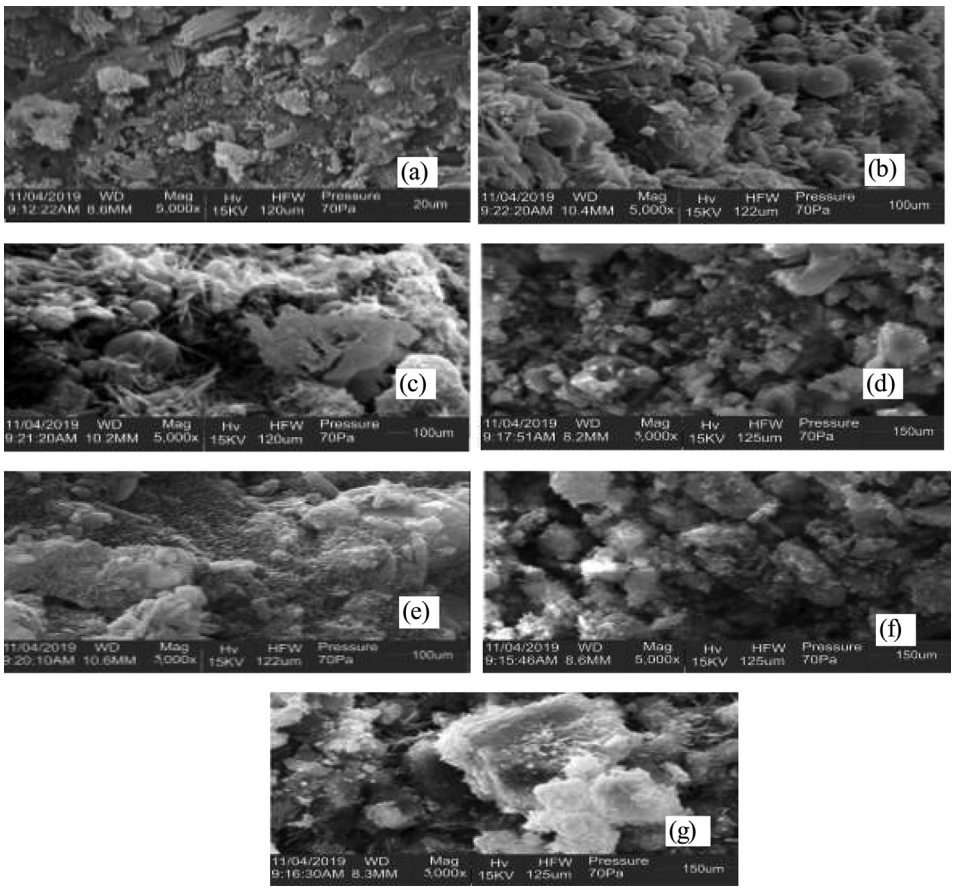

Fig. 8. SEM micrographs of M 40 on (a) 100% PCC, (b) 100% GGBFS, (c) 80% GGBFS + 20% CCA, (d) 60% GGBFS + 40% CCA, (e) 40% GGBFS + 60% CCA, (f) 20% GGBFS + 80% CCA, and (g) 100% CCA.

morphological appearance. The partially reacted and unreacted CCA particles are ordinarily shown in G6, as revealed by SEM micrographs in Fig. 8 (g).

The EDX for M 40 (100% PLC), as indicated in Fig. 9, showed the different chemical compositions and phases in the mix. The presence of calcium, silicon, aluminium, sodium, carbon, oxygen and iron were confirmed in the EDX analysis. It was obvious that calcium, silicon, and oxygen were the major chemical species present in the mix. Calcium gained 0.98 counts per second per electron-volt (cps/eV) in one kilo electron-volt (keV) while silicon gained 1.0, 0.77, and 0.30 cps/eV in the range of 1.4 to 2.2 keV. The presence of silicon in the mix may be attributed to the fraction of aggregates [49]. The EDX analysis for GPC 1 (100% GGBFS), as shown in Fig. 9, confirmed the presence of calcium, silicon, aluminium, carbon, oxygen and iron in the mix having calcium, iron, silicon, and oxygen as the main chemical elements in a high cps/eV at keV. Also, the presence of silicon is attributed to the aggregates available in the mix. It was clearly noticed from the EDX analysis that the intensity of calcium counts in GPC 1 (100% GGBFS) was higher than those obtained for M 40 (100% PLC) and GPC 6 (100% CCA). The reason for higher calcium counts could be attributed to the fact that unlike PLC, most of CaO present in GGBFS is tied up as calcium silicate, calcium aluminate, and calcium aluminosilicate, because GGBFS is 100% glassy [8]. The EDX analysis for GPC 6 (100% CCA), as shown in Fig. 9, has negligible calcium counts, which may be mainly responsible by sodium aluminosilicate hydrate (N-A-S-H) [41,89], hence resulting in the cosmetic product rather than binding product [78]. Therefore, the lowest strength observed for G6 (100% CCA) may be linked to the formation of N-A-S-H and lesser microstructure in the mixture [89]. Besides, the intensity of silicon counts in GPC 6 (100% CCA) was higher than that of M 40 (100% PLC) and GPC 1 (100% GGBFS); this may be associated with the higher percentage of SiO2 content obtained for CCA, as shown in Table 4, as well as component of aggregates in the mix.

3.4.2. Morphological analysis

The results of the morphological analysis conducted on the selected concrete samples, PCC, G1 and G6 at 7 and 28 days of hydration are shown in Fig. 10. The morphology of PCC, as respectively shown in Fig. 10 (a) and (b) for 7 and 28 days of hydration, indicated a better interface condition but there was a sign of pores at 28-day which may not apparently have a major effect on the mechanical properties of the concrete. Therefore, the morphology signified an adequate compact and uniform matrix between the constituent particles and the cementitious matrix [91]. On the other hand, a better interface nature was also observed for G1 as shown in Fig. 10 (c) and (d) for 7 and 28 days respectively. Although, the SEM micrograph at 28-day revealed some micropores which apparently had no major effect on the mechanical properties of the concrete. The morphology, therefore, could be classified as a compact which signified a uniform matrix between the constituent particles and the cementitious matrix [91]. However, the morphology of G6 in Fig. 10 (e) and (f) showed a surface of a non-refined pattern at 28-day. In addition, micropores were noticed. Therefore, the morphology showed a lesser cohesive structure, and SEM-EDX analysis revealed insignificant counts of calcium, hence attributing to its lesser mechanical performances compared with PCC and G6.

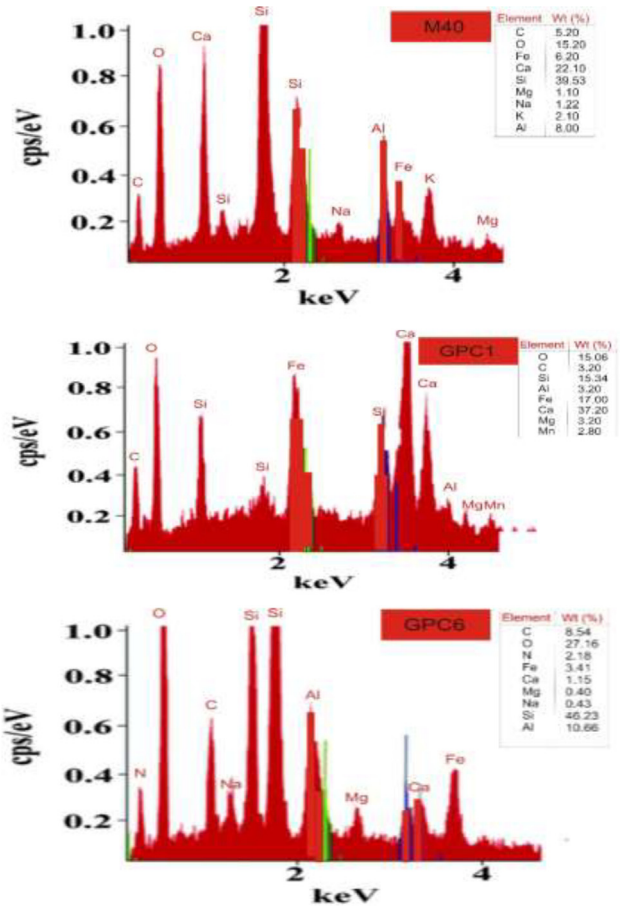

Fig. 9. EDX analysis on M 40 (100% PCC), GPC 1 (100% GGBFS), and GPC 6 (100% CCA).

3.4.3. XRD analysis

The results of XRD patterns acquired by a scanning rate of 1 degree per minute from 0 to 60 degrees (2θ) after 28-day of hydration for the selected concrete samples are illustrated in Fig. 11. In Fig. 11 (a), the quartz (amorphous phases) exhibited a broad shoulder of 82.98% at 27° of 2θ value for the PCC sample. The peak of this quartz phase is attributed to the component of aggregates in the mix [49,92]. The XRD analysis also displayed the peaks of calcium hydroxide (Portlandite) with the percentage constituents of 1.25% owing to cementitious reactions. In addition, the exhibition of calcite ($CaCO_3$) showing 12.57% may be attributed to the reaction between the alkali carbonate and portlandite ($Ca(OH)_2$) in the mix, thus resulting in the precipitation and inducement of the paste rigidity [49]. The chemical reaction between silicon oxide (SiO_2) and $Ca(OH)_2$ produced the hydration product of cement; and the hydration product of cement resulted in the C-S-H [49,93,94]. Moreover, the diffraction peak for C-S-H from the XRD analysis was noticed at diffraction angle 2θ, equaling 21° to 60°. Therefore, the hardened product of the PCC may be attributed to the reaction of the hydration products such as C-S-H and Ca $(OH)_2$ which majorly comprise silica and calcium contents [49,91].

The XRD pattern of reaction products for G1 containing 100% GGBFS is shown in Fig. 11 (b), and the broad shoulders were revealed. The quartz phase showed a diffraction peak of 66.85% at 27^0 of 2θ. The peak of quartz phase is attributed to the component of aggregates in the mix [49,92]. Also, the XRD analysis revealed the diffraction of calcium carbonate (calcite) with 15.77%. This may be due to the fact that GGBFS exhibits both cementitious and pozzolanic properties, and these properties, in the presence of alkaline activators, results in $CaCO_3$. Moreover, unlike PLC with C_3S (alite), C_2S (belite) and C_3A (aluminate cubic or ortho), almost all CaO (Lime) found in GGBFS is kept occupied as calcium aluminate, calcium silicate, and calcium aluminosilicate because GGBFS is almost 100% glassy [17,18,94]. The XRD spectrum also revealed a higher periciase (MgO) content of 1.42% compared with 0.86% and 0.40% for PCC and G6, respectively. This may be attributed to the more glassy content in GGBFS compared with PLC and CCA. It is reported that MgO (≤2%) in the mix significantly contributes to the soundness and strength gain of concrete [49]. Furthermore, apart from the formation of geopolymer gel, Davidovits [17], Fernandez-Jimenez et al. [18], Temuujin et al. [83], and Xu and Deventer [95] opined that the chemical reaction of calcium in the mix with silicate and aluminate monomers which dissolve from GGBFS or pozzolan results in the formation of both C-S-H and C-A-S-H. Consequently, it contributes to the higher mechanical strength of the hardened matrix, improves the polymerization process, and significantly contributes to the mechanical strengths, hence attributing to the higher mechanical strength of GGBFS-CCA based GPC than that of the PCC. During the dissolution process, the glassy phase of aluminosilicates present in the GGBFS or pozzolan chemically reacts with the alkaline solutions and results in x-ray amorphous aluminosilicate gel (X-RAAG). In addition, Davidovits [17], Fernandez-Jimenez et al. [18], and Xu and Deventer [90] reported that x-ray amorphous aluminosilicate gel is credited for the cementitious nature of the final material and its quality affects the strengths of the hardened product. Therefore, the presence of amorphous hump from the XRD analysis was noticed at diffraction angle 2θ, equaling 21° to 60°, and this can be attributed to the presence of amorphous glassy in the mixture [96].

The XRD pattern of reaction product for G6 containing 100% CCA is shown in Fig. 11 (c). The XRD spectrum exhibited a ferrite (C_4AF) at 0.56% compared with PCC and G1 samples which possessed none. This compound acts as a flux and reduces the burning temperature of corncob, thus facilitating the combination of silica and lime in the CCA [49]. However, the exhibition of calcium sulfate hemihydrate ($Ca_2H_2O_9S_2$) with 2.14% indicated a false set in the mix, hence improving the workability of the mix properties and slowing down the strength gain [49]. On the other hand, the presence of calcium sulfate dihydrate (CaH_4O_6S) of 1.61% in the XRD spectrum facilitates the strength development. The XRD pattern for G6, unlike G1 with an amorphous structure, indicated the presence of a crystalline structure, resulting in low reactivity of pozzolanic reactions. This was in line with Neville [49] that amorphous silica is more beneficial than the crystalline silica in that it is much more reactive in pozzolanic reactions, hence confirming the low strength performance of G6 compared with that of G1 and other mixtures. In addition, the exhibition of potassium sulfate (K_2S) in the XRD spectrum with 7.22% may be attributed to the soluble-alkali in the mix, and this reduces the strength gain [49]. Above all, it can be inferred that the combination of both CCA and GGBFS results in the formation of ternary gels, C-S-H, C-A-S-H and N-A-S-H, hence leading to the improvement of mechanical strengths of the produced GPC.

3.5. Prediction of mechanical strengths

3.5.1. Relationship between splitting tensile strength (STS) and compressive strength (CS)

Following the model equations illustrated in Table 3 [65–70], the proposed model for the relationship between STS and CS of GGBFS based GPC incorporated with CCA is shown in Fig. 12. Moreover, the model equation is proposed for the range of 15 to 65 MPa of mean CS, hence the proposed model equation is shown in Eq. (1).

$$fct = 0.6628fc^{0.4837} \quad (1)$$

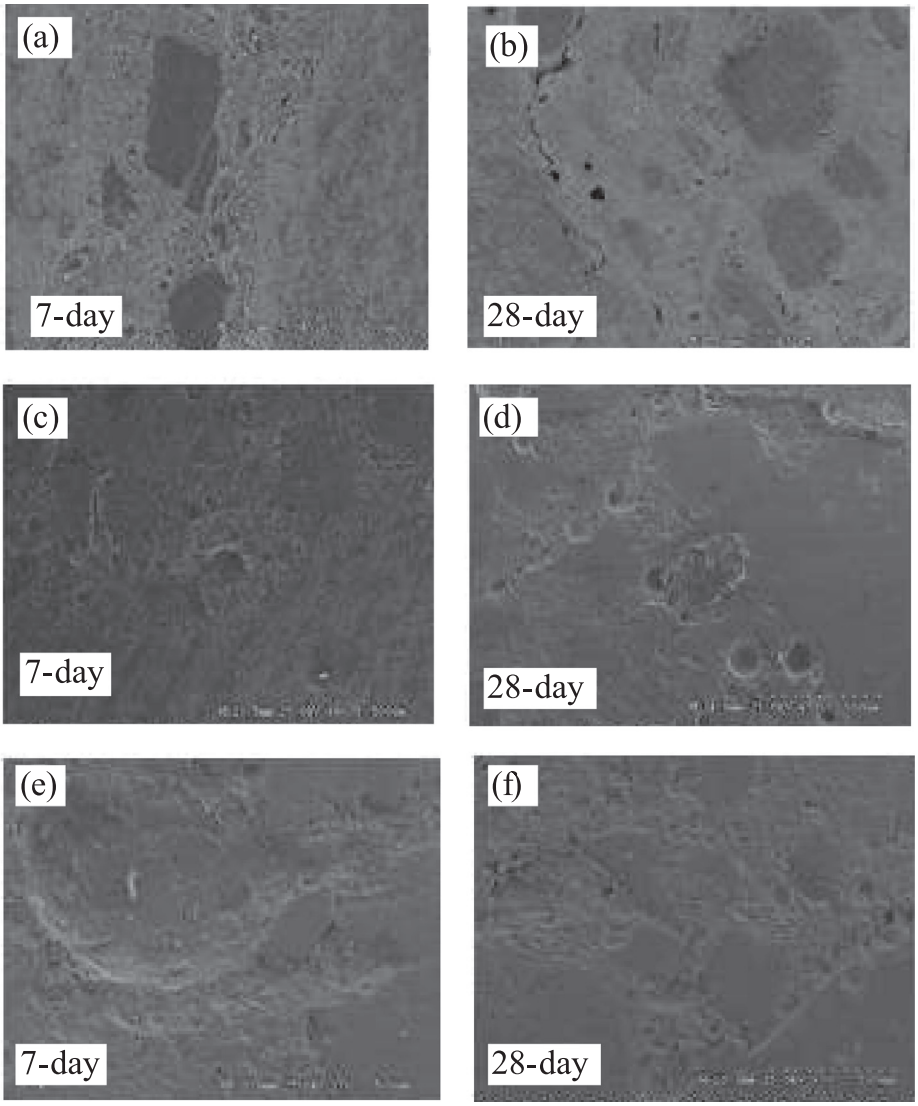

Fig. 10. Morphology on (a) and (b) 100% PCC, (c) and (d) 100% GGBFS, and (e) and (f) 100% CCA, for 7 and 28 days, respectively.

where fct is the STS of GPC (in MPa)
fc is the CS of GPC (in MPa)

The relationship between the STS and the CS of GPC, as shown in Fig. 12, revealed that the coefficient of determination (R^2) for the model was 95.34% fit to predict the relationship at 95% confidence bound of CS. The prediction is similar to BS EN 1992-1:1 [67] whose coefficient of determination (R^2) for the relationship between the STS and the CS was 96.8%. Therefore, it is concluded that this proposed model equation can be suitably used to forecast the strength development of GPC incorporating agro-industrial wastes in the range of 15 to 65 MPa of CS.

3.5.2. Relationship between flexural strength (FS) and CS

As indicated in Table 3, the proposed model for the relationship between FS and CS is illustrated in Fig. 13, while the equation is shown in Eq. (2). Similarly, the model equation is proposed for the range of 15 to 65 MPa of mean CS.

$$fr = 0.8271fc^{0.5271} \quad (2)$$

where fr is the FS of GPC (in MPa)
fc is the CS of GPC (in MPa)

As illustrated in Fig. 13, the relationship between FS and CS of GPC indicated that the coefficient of determination (R^2) for the model was 98.10% fit to predict the relationship at 95% confidence bound of CS. This prediction is also similar to BS EN 1992-1:1 [67] whose coefficient of determination (R^2) for the relationship between FS and CS was 97.20%. Therefore, it is concluded that this proposed model equation can be beneficial in the forecast of flexural strength development for GPC incorporating agro-industrial wastes ranging from 15 to 65 MPa of CS.

3.6. Validation of experimental models with different model equations

3.6.1. STS and CS

The determination of correlation between STS and CS of GPC has neither been specified nor developed in concrete codes. Moreover, the key parameters in the analysis and design of concrete structural members are the STS and the CS [49,65,67]. Following the

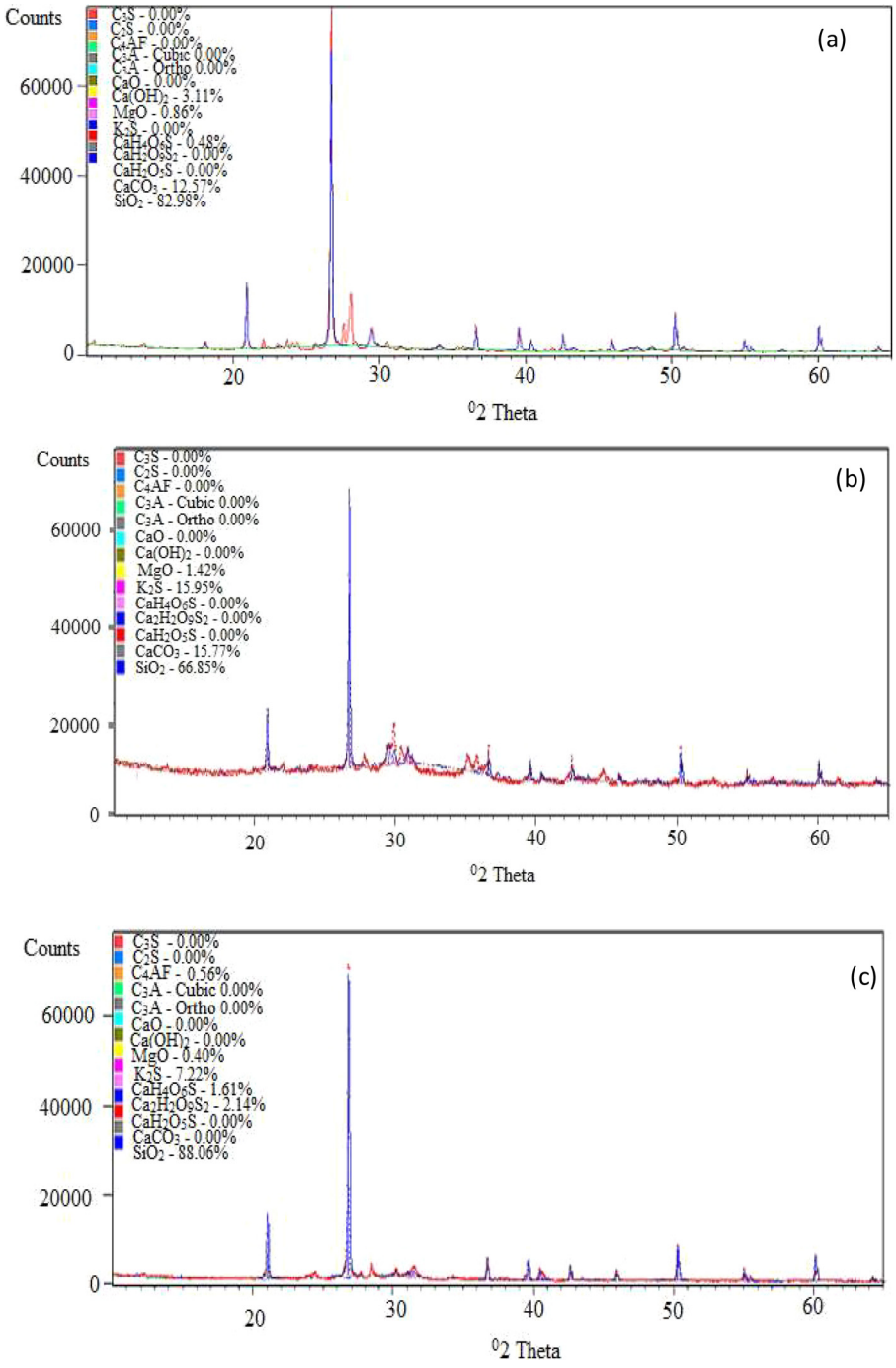

Fig. 11. XRD spectra (a) PCC (100% PLC) (b) G1 (100% GGBFS) and (c) G6 (100% CCA).

previous model equations presented in Table 3 [65–70] and the experimental model equation (Eq. (1)), the validation of STS from different model equations at 28 days is shown in Fig. 14 (a) and (b) for both M 30 and M 40, respectively.

It was revealed in Fig. 14 (a) that the STS for all concrete types increased with increasing CS in the same trend. Moreover, the trend also illustrated that both the experimental value and the developed model from this study were significantly correlated. In furtherance of the trend from Fig. 14 (a), Tempest [69] and Lavanya and Jegan [70]'s model equations were closely situated to the data points of experimental value and model at the lower range of CS. However, there was a wider gap in the higher range of CS. This supported the finding of Neupane [66] that Tempest [69] and Lavanya and Jegan [70]'s model equations are closely situated to the experimental value of GPC in the range of CS but there is a higher gap in high strength range. Contrarily, BS EN 1992-1:1[67]'s model equation forecast a lower STS at both lower and higher ranges of CS, compared with both the experimental value and model. Moreover, Neupane [66]'s model equation estimated a higher STS at both lower and higher ranges of CS, compared with the experimental value and model. Furthermore, comparing with both the experimental value and model, AS 3600 [65] and Sofi et al. [68]'s model equations estimated a lower STS at both lower and higher ranges of CS. These results established that Tempest [69] and Lavanya and

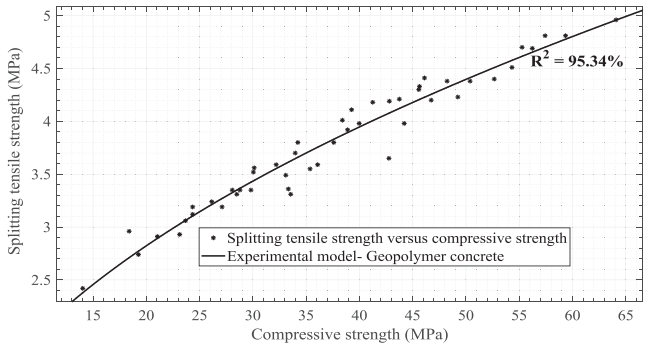

Fig. 12. Correlation of STS and CS of GPC.

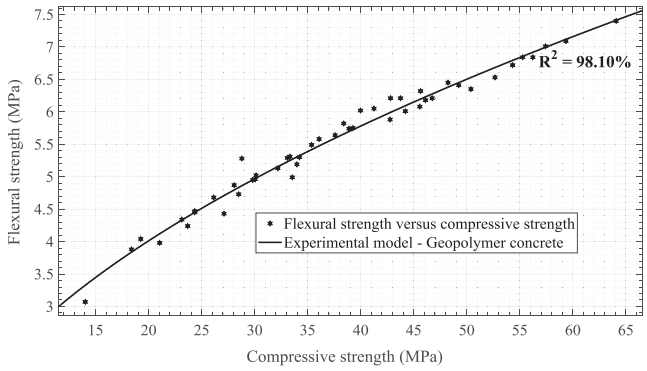

Fig. 13. Correlation of FS and CS of GPC.

Jegan [70]'s model equations validated both the experimental value and the developed model equation of this study at the lower range of CS. The differences in the validation may be attributed to the type of mix proportion, the difference in chemical compositions of source materials and liquid contents used in the production of the concretes [49].

The STS for all concrete types increased with increasing CS in a similar trend, as illustrated in Fig. 14 (b) for M 40. It was also illustrated from the trend that the experimental value and the model were significantly correlated. Lavanya and Jegan [70]'s model equation was closely located to the data points of experimental value at the lower range of CS; however, there is a wider margin at the higher range of CS. This trend also confirmed the finding of Neupane [66] that Lavanya and Jegan [70]'s model equation is closely situated to the experimental value of GPC in the lower range of CS but there is a higher margin in high strength range. Besides, Tempest [69]'s model equation was nearly located to the experimental value at the higher range of CS, but there is a higher gap at the lower range of CS. Moreover, BS EN 1992-1:1 [67]'s model equation was closely located to the data points of the experimental value and model at both lower and higher ranges of CS. In addition, Neupane [66]'s model equation estimated a higher STS at both lower and higher ranges of CS, compared with the experimental value and model. Comparing with both the experimental value and model, the AS 3600 [65] and Sofi et al. [68]'s model equations also estimated a lower STS at both lower and higher ranges of CS. Therefore, these results established that BS EN 1992-1:1 [67]'s model equation validated the experimental value and model of this study at both lower and higher ranges of CS. Lavanya and Jegan [70]'s model equations validated the experimental value at the lower range of CS while Tempest [69]'s model equation validated the experimental value at the higher range of CS. The difference in model validation may be associated with the difference in chemical compositions of source materials and liquid contents used in the production of GPC [49]. Ultimately, the proposed model equation developed from this study can also be suitably applied in the strength prediction of PCC incorporating agro-industrial wastes, because it validated BS EN 1992-1:1 [67]'s model equation established for PCC at both lower and higher ranges of CS.

3.6.2. FS and CS

Similar to STS, there is no available equation recommended in concrete standards to relate both FS and CS of GPC. In addition, FS plays a vital parameter in the design and analysis of concrete structural members [49,63,65]. Therefore, conforming to Table 3 [63–69] and Eq. (2), the validation of FS from different model equations are presented in Fig. 15 (a) and (b) for both M 30 and M 40 at 28 days of curing, respectively.

It was indicated in Fig. 15 (a) that the FS for all concrete types increased with increasing CS in the same trend. The experimental model and value were significantly correlated. Furthermore, Neupane [66]'s model equation was closely located to the data points of experimental value at both lower and higher ranges of CS. The BS EN 1992-1:1 [67]'s model equation was nearly located to the experimental value at the higher range of CS, but there is a higher gap at the lower range of CS. Moreover, comparing with the experimental value, AS 3600 [65], Sofi et al. [68] and Diaz-Loya et al. [71]'s model equations estimated a lower FS at both lower and higher ranges of CS. Therefore, these results proved that the Neupane [66]'s model equation validated the experimental value at both lower and higher ranges of CS. Moreover, the BS EN 1992-1:1 [67]'s model equation validated the experimental value and model at the higher range of CS.

Similar to the trend of M 30 in Fig. 15 (a), the FS for all concrete types increased with increasing CS in the same trend as shown in Fig. 15 (b) for M 40. Neupane [66]'s model equation was closely located to the data points of experimental value at both lower and higher ranges of CS. Contrarily, BS EN 1992-1:1 [67]'s model equation was nearly located to the experimental value at the higher range of CS, but there is a higher gap at the lower range of CS. Comparing with the experimental value and model, the AS 3600 [65], Sofi et al. [68] and Diaz-Loya et al. [71]'s model equations estimated a lower FS at both lower and higher ranges of CS. The results, therefore, asserted that Neupane [66]'s model equation validated the experimental value at both lower and higher ranges of CS. However, the BS EN 1992-1:1 [67]'s model equation validated both the experimental value and model at the higher range of CS. Therefore, the proposed model equation developed from this study can also be suitably applied in the strength prediction of PCC incorporating agro-industrial wastes, because it validated Neupane [66]'s model equation established for PCC, at both lower and higher ranges of CS.

3.7. Validation of proposed model equations with different experimental results from other studies

Table 5 presents the validation of the proposed model equations with other experimental results to examine the accuracy and validity of the equations at 28 days curing following the relationships, as illustrated in Eqs. (1) and (2).

The statistics, as shown in Table 5, indicated that the predicted values by the proposed model equations were 9% to 19%, 0% to 7%, 5% to 13%, and 1% to 16% higher than the experimental results obtained by Deb et al. [37], Jain [98], Vijai et al. [99], and Nath and Sarker [100] for STS, FS, FS, and FS, respectively. However, a 0% to 8%, 18%, 2% to 4%, and 2% to 16% increase in the predicted values using the proposed model equations were obtained compared with the exxperimental results obtained by Deb et al. [37], Basir [97], Jain [98], and Nath and Sarker [100] for STS, STS and FS, FS,

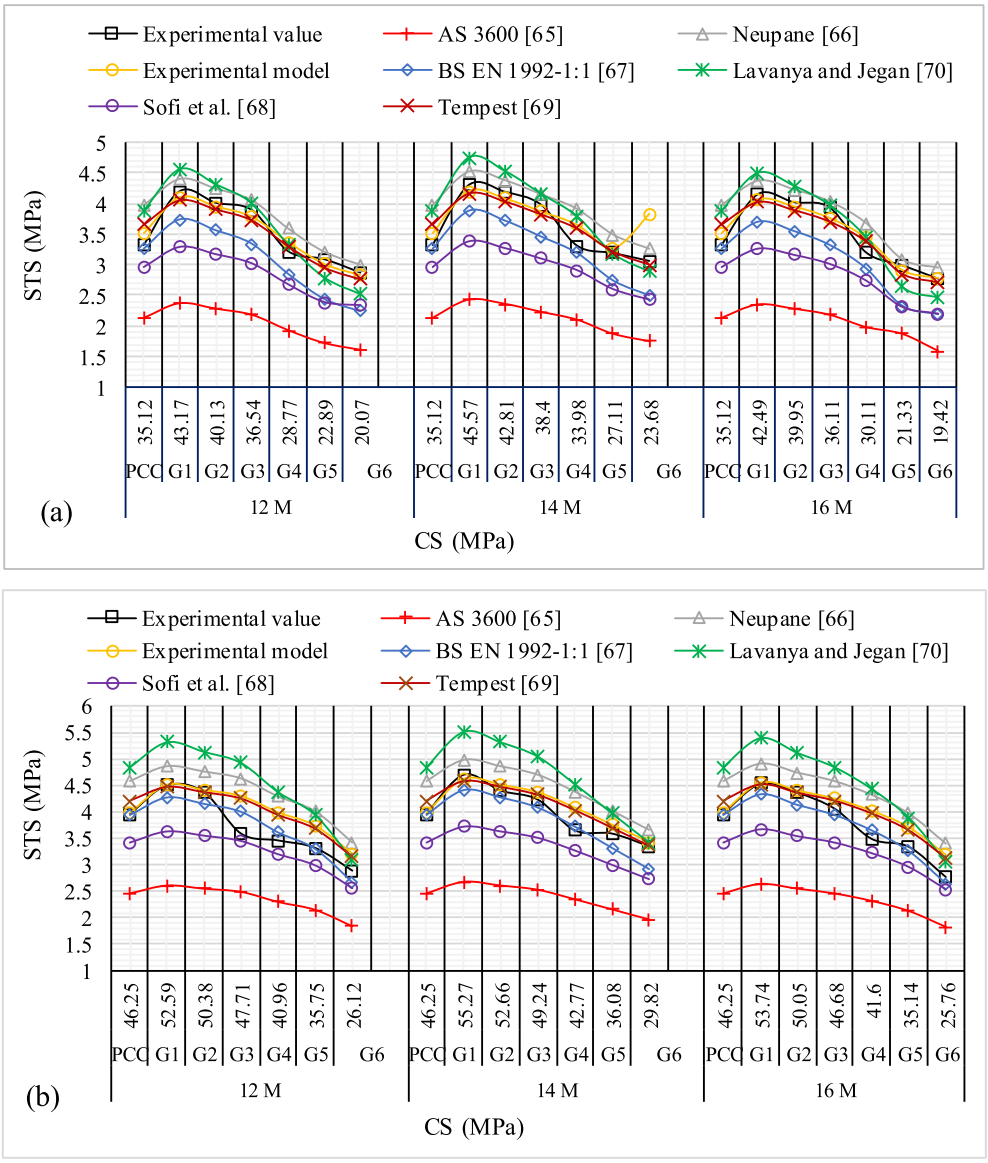

Fig. 14. Validation of experimental STS model with different model equations for (a) M 30 and (b) M 40 at 28 days curing.

and FS, respectively. Comparing the predicted values by the proposed model equations with the previous exprimental results [37,97–100], no significant difference was noticed owing to the variability of the mix compositions. Therefore, the model equations proposed by this study can be applied for GPC cured at ambient condition with reasonable margin of factor of safety.

4. Conclusion

The study investigated the mechanical strengths, microstructures and mineralogical phases of GGBFS-CCA based GPC using M 30 and M 40 as mix design proportions, and SH solution and SS gel as alkaline activators. In the course of the study, both experimental and statistical methods were used and the results were compared with PCC. Based on these extensive investigations and in consonance with the research aims, the following sets of conclusions are made:

- The compressive strength, flexural strength and splitting tensile strength of GGBFS-CCA based GPC was higher than that of PCC. However, the optimum replacement level for both GGBFS and CCA to exhibit the higher mechanical strengths compared with PCC was found to be 60% GGBFS and 40% CCA at all levels of molar concentrations for both M 30 and M.
- The 14 M of SH solution achieved the highest compressive, flexural, and splitting tensile strengths at all levels of GPC mixes for both M 30 and M 40. Moreover, a marginal increase was observed for 12 M compared with that of 16 M.
- Both flexural and splitting tensile strength of GGBFS-CCA based GPC increased with increasing compressive strength at all levels of molar concentrations for both M 30 and M 40.
- The SEM micrographs for GGBFS-CCA based GPC samples indicated an amorphously structured matrix in spherical flakes with sharp needles. Furthermore, a better interface pattern was observed for the morphology of GGBFS-CCA based GPC samples at 28-day, signifying a good compact, uniform matrix and fewer pores.

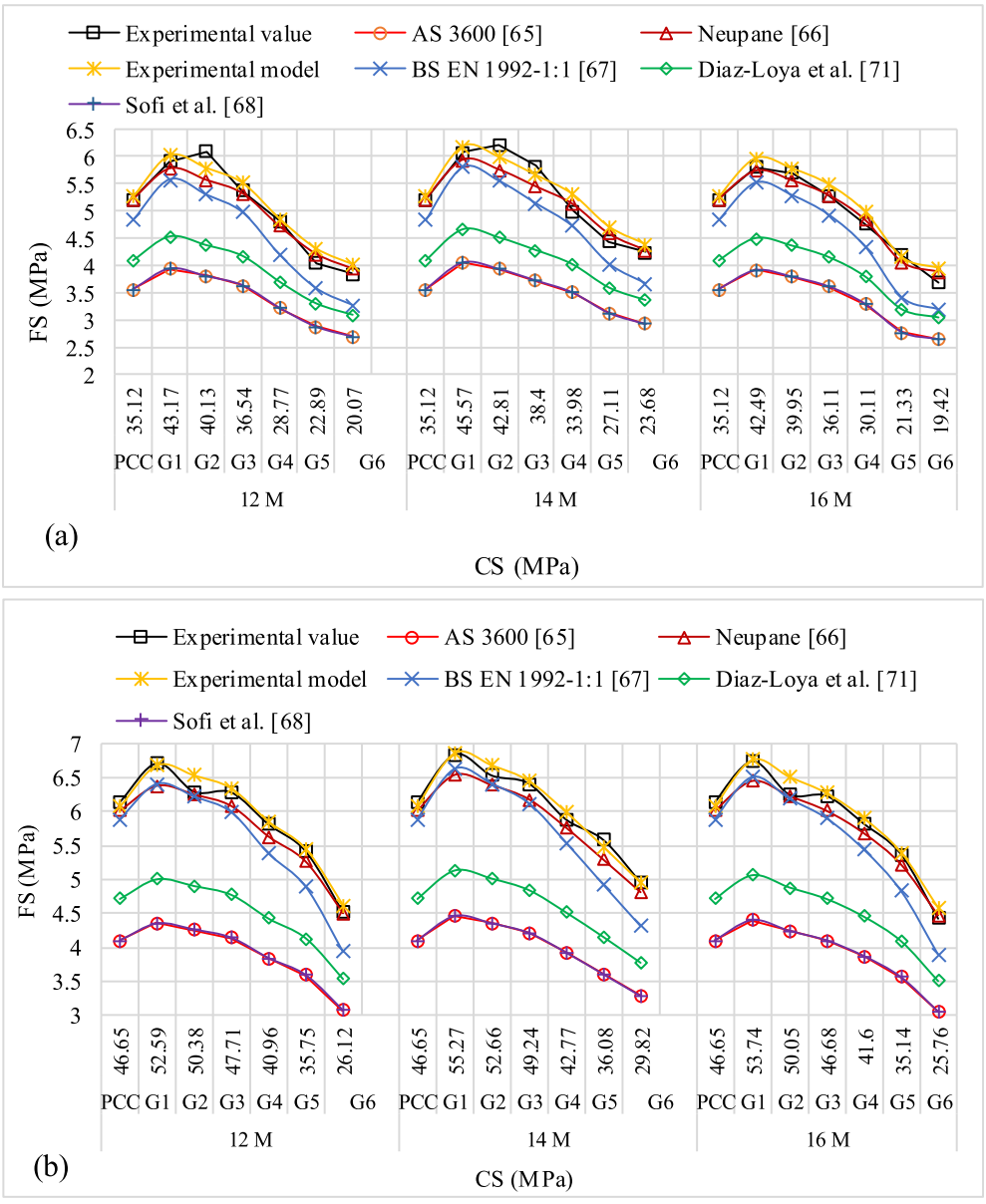

Fig. 15. Validation of experimental FS model with different model equations for (a) M 30 and (b) M 40 at 28 days curing.

- The XRD spectra of GGBFS-CCA based GPC indicated Quartz and calcite as the major chemical compounds which were kept occupied as calcium aluminate, calcium silicate, and calcium aluminosilicate, and consequently, formed the C-A-S-H gel that improved the mechanical strengths of GPC.
- There was a good correlation between the experimental results and the proposed model equations.

The production of GPC incorporating CCA and GGBFS as agro-industrial wastes at ambient curing conditions is attainable for the production of low and normal strength concrete. This study benefits future research and the technological development of GPC by concentrating on three prospective solutions. First, it can harness and recycle agro-industrial by-products thereby reducing the number of harmful materials indiscriminately disposed as wastes. Second, it can be utilized as a new alternative SCM, which possess a lower carbon footprint than the PCC. Third, the proposed models available therein can be useful in the prediction and application of strength design proportions for GPC incorporating agro-industrial by-products under ambient curing conditions.

CRediT authorship contribution statement

Solomon Oyebisi: Conceptualization, Data curation, Formal analysis, Funding acquisition, Investigation, Software, Methodology, Writing - original draft. **Anthony Ede:** Project administration, Resources, Supervision, Validation, Writing - review & editing. **Festus Olutoge:** Project administration, Resources, Supervision, Validation, Writing - review & editing. **David Omole:** Validation, Writing - review & editing.

Declaration of Competing Interest

The authors declare that they have no known competing financial interests or personal relationships that could have appeared to influence the work reported in this paper.

Table 5
Validation of the proposed model equations at 28 days curing.

Source	Mix ID	f_c (MPa)	f_r (MPa)	f_{ct} (MPa)	Validation		% Difference	
					$f_r = 0.8271f_c^{0.5271}$(MPa)	$f_{ct} = 0.6628f_c^{0.4837}$ (MPa)	f_r	f_{ct}
Deb et al. [37]	&10% G + 90% FA	37	–	3.09	–	3.80	–	+19%
	&20% G + 80% FA	44	–	3.75	–	4.13	–	+9%
	*10% G + 90% FA	40	–	3.48	–	3.95	–	+12%
	*20% G + 80% FA	41	–	4.81	–	4.44	–	−8%
Basir [97]	&100% FA: 12 M	24.65	5.43	3.83	4.48	3.12	−18%	−18%
	&100% FA: 14 M	25.73	5.60	3.91	4.58	3.20	−18%	−18%
Jain [98]	5% G + 95% PLC	33.20	4.85	–	5.24	–	+7%	–
	10% G + 90% PLC	34.75	4.97	–	5.37	–	+7%	–
	15% G + 85% PLC	34.67	5.56	–	5.36	–	−4%	–
	20% G + 80% PLC	34.69	5.49	–	5.36	–	−2%	–
	25% G + 75% PLC	34.12	5.33	–	5.33	–	0%	–
Vijai et al. [99]	&100% FA: 12 M	25.63	4.00	–	4.57	–	+13%	–
	&100% FA: 16 M	19.71	3.80	–	3.98	–	+5%	–
Nath and Sarker [100]	&100% FA[a]	25.60	4.89	–	4.57	–	−7%	–
	&90% FA+10% G[a]	38.30	5.79	–	5.65	–	−2%	–
	&85% FA+15% G[a]	46.60	5.26	–	6.27	–	+16%	–
	&100% FA[b]	32.50	6.13	–	5.18	–	−16%	–
	&90% FA+10%G[c]	33.30	4.27	–	5.25	–	+11%	–
	&94% FA+6% PLC[a]	43.20	6.42	–	6.02	–	−6%	–
	&97% FA+3% PLC[a]	34.40	5.54	–	5.34	–	−4%	–
	&94% FA+6% PLC[c]	35.30	6.06	–	5.41	–	−11%	–
	&98% FA+2% CH[a]	42.00	6.32	–	5.93	–	−6%	–
	&97% FA+3% CH[a]	41.50	5.83	–	5.89	–	+1%	–
	&98% FA+2% CH[c]	36.80	5.93	–	5.53	–	−7%	–

a is water/solid (w/s) of 0.202; b is w/s of 0.180; c is w/s of 0.193.
& represents the mix ratio of SS/SH = 2.5:1; * denotes the mix ratio of SS/SH = 2:1; G is GGBFS; CH is $(Ca(OH)_2)$;

Acknowledgements

The researchers appreciate the Covenant University Centre for Research, Innovation, and Discovery (CUCRID) for the provision of the fund and conducive environment in the course of this study.

References

[1] A. Bouaissi, L. Li, M. Abdullah, Q. Bui, Mechanical properties and microstructure analysis of FA-GGBS-HMN based geopolymer concrete, Constr. Build. Mater. 210 (2019) 198–209.
[2] V.M. Malhotra, Introduction: sustainable development and concrete technology, Concr. Int. 24 (7) (2002) 22.
[3] United Nations Environment Programme, Emissions Gap Report, UNEP, 2016. ISBN: 978-92-807-3617-5.
[4] United Nations Environment Programme, A UNEP Synthesis Report, UNEP, 2017. ISBN: 978-92-807-3617-5.
[5] Emission Database for Global Atmospheric Research, Global CO2 Emissions from Fossil Fuel Use and Cement Production 1970-2015, EDGAR. http://edgar.jrc.ec.europe.eu/, version 4.3.2, 2016 (accessed 18 August 2019).
[6] International Energy Agency- Energy Technology Systems Anal Programme, Cement Production, IEA ETSAP - Technology Brief 103. www.etsap.org.investment/, 2015 (accessed 10 August 2019).
[7] British Geological Survey, Cement Raw Materials, Natural Environment Research Council. Retrieved from https://www.bgs.ac.uk/downloads/start.cfm?id=1408, 2005 (accessed 5 August 2019).
[8] J. Davidovits, Geopolymer cement: A Review. http://www.geopolymer.org/library/technical-papers/21-geopolymer-cement-review, 2013 (accessed 24 April 2019).
[9] D. Hardjito, S.E. Wallah, D.M. Sumajouw, B.V. Rangan, Development of fly ash-based geopolymer concrete, ACI. Mater. J. 101 (6) (2004) 55–64.
[10] United States Geological Survey, Mineral Commodity Summaries, USGS Reports, 2017. Retrieved from https://minerals.usgs.gov/minerals/pubs/mcs/2017/mcs2017.pdf, 2017 (accessed 29 December 2018).
[11] World Health Organization, World Health Statistics, WHO, Geneva, 2016.
[12] Sustainable Development Goals, Transforming Our World: The 2030 Agenda for Sustainable Development, Report of the United Nations Statistics Division. https://unstats.un.org/sdgs, 2015 (accessed 5 April 2019).
[13] Sustainable Development Goals, The Sustainable Development Goals Report of the United Nations Statistics Division, United Nations Publication issued by the Department of Economic and Social Affairs (DESA), New York, NY, 10017, United States of America. https://unstats.un.org/sdgs, 2017 (accessed 27 July 2019).
[14] B. Jim, B. Steve, E. Pepke, J. Howe, F. Kathryn, G. Harry, Atmospheric Carbon Dioxide and Premature Deterioration of Steel-Reinforced Concrete Structures – a Growing Concern. A Trusted Source of Environmental Information, Dovetail Partners Inc. Hennepin Ave, Minneapolis, MN55403, 2016.
[15] P.K. Mehta, R.W. Burrows, Building durable structures in the 21st century, ACI. Concr. J. 23(3), 57-63.
[16] N. Subramanian, How to guarantee design-life of concrete structures, The Master Builder (2016) 1–23.
[17] J. Davidovits, Geopolymer Chemistry and Applications, Institut Géopolymère, 3rd ed., Saint-Quentin, France, 2008.
[18] A. Fernandez-Jimenez, I. Gracia-Loderio, A. Palomo, Durability of alkali-activated fly ash cementitious materials, J. Mater. Sci. 42 (2007) 3055–3065.
[19] B.V. Rangan, Low-Calcium Fly Ash-Based Geopolymer Concrete, Concrete Construction Engineering Handbook (Chapter 26). Editor-in-Chief E.G. Nawy, 2nd ed., CRC Press, New York, 2008.
[20] B. Rangan, Fly Ash-Based Geopolymer Concrete, Allied Publishers Private Limited, Mumbai-India, 2010, pp. 66–108.
[21] T.A. Aiken, J. Kwasny, W. Sha, M.N. Soutsos, Effect of slag content and activator dosage on the resistance of fly ash geopolymer binders to sulfuric acid attack, Cem. Concr. Res. 111 (2018) 23–40.
[22] S. Oyebisi, A. Ede, F. Olutoge, O. Ofuyatan, J. Oluwafemi, Influence of alkali concentrations on the mechanical properties of geopolymer concrete, Int. J. Civ. Eng. Technol. 9 (8) (2018) 734–743.
[23] S. Oyebisi, A. Ede, F. Olutoge, O. Ofuyatan, O.J. Oluwafemi, Modeling of hydrogen potential and strength of geopolymer concrete, Int. J. Civ. Eng. Technol. 9 (7) (2018) 671–679.
[24] S. Oyebisi, A. Ede, O. Ofuyatan, T. Alayande, G. Mark, J. Jolayemi, S. Ayegbo, Effects of 12 molar concentration of sodium hydroxide on the compressive strength of geopolymer concrete, IOP Conf. Series: Mater. Sci. Eng. 413 (2018), https://doi.org/10.1088/1757-899X/413/1/012066 012066.
[25] S. Oyebisi, J. Akinmusuru, A. Ede, O. Ofuyatan, G. Mark, J. Oluwafemi, 14 molar concentrations of alkali-activated geopolymer concrete, IOP Conf. Series: Mater. Sci. Eng. 413 (2018), https://doi.org/10.1088/1757-899X/413/1/012065 012065.
[26] S. Oyebisi, A. Ede, F. Olutoge, O. Ofuyatan, T. Alayande, Building a sustainable world: Economy index of geopolymer concrete, 10th Int. Struct. Eng. Constr. Conf. (ISEC-10), 2019. ISBN: 978-0-9960437-6-2.
[27] J. Kamau, A. Ahmed, P. Hirst, J. Kangwa, Suitability of corncob ash as a supplementary cementitious material, Int. J. Mater. Sci. Eng. 4 (4) (2016) 215–228.
[28] S.O. Oyebisi, F.A. Olutoge, M.O. Ofuyatan, A.A. Abioye, Effect of corncob ash blended cement on the properties of lateritic interlocking, Prog. Ind. Ecol. Int. J. 11 (4) (2017) 373–387.
[29] S. Oyebisi, A. Ede, O. Ofuyatan, J. Oluwafemi, I. Akinwumi, Comparative study of corncob ash-based lateritic interlocking and concrete hollow blocks, Int. J. Geomate 15 (51) (2018) 209–216, https://doi.org/10.21660/2018.51.45918.
[30] S. Oyebisi, A. Ede, F. Olutoge, T. Igba, J. Ramonu, Rheology of slag-based geopolymer concrete using corncob ash as a pozzolanic material, IOP Conf. Series: Mater. Sci. Eng. 640 (2019), https://doi.org/10.1088/1757-899X/640/1/012057 012057.
[31] S. Oyebisi, A. Ede, F. Olutoge, T. Igba, J. Oluwafemi, Effects of rest period on the strength performance of geopolymer concrete, IOP Conf. Series: Mater. Sci. Eng. 640 (2019), https://doi.org/10.1088/1757-899X/640/1/012056 012056.

[32] A.A. Raheem, S.O. Oyebisi, S.O. Akintayo, M.O. Oyeniran, Effects of admixture on the properties of corncob ash cement concrete, Leonardo Electron. J. Pract. Technol. 16 (2010) 13–20.
[33] A.A. Raheem, D.A. Adesanya, A study of thermal conductivity of corn cob ash blended cement mortar, Pacific J. Sci. Technol. 12 (2) (2011) 106–111.
[34] S. Oyebisi, T. Igba, D. Oniyide, Performance evaluation of cashew nutshell ash as a binder in concrete production, Case Studies Constr. Mater. 11 (2019) e00293.
[35] G.I. Obiefuna, P.H. Sini, A. Maunde, Geochemical and mineralogical composition of granitic rock deposits of Michika area North East, Nigeria, Int. J. Sci. Technol. Res. 7 (4) (2018) 160–170.
[36] A. Rittman, Using the Rittman serial index to define the alkalinity of igneous rocks, E Schwetzerbartsche Vealagsbuchandlung Stuttgart 184 (1) (1962) 95–103.
[37] P.S. Deb, P. Nath, P.K. Sarker, Properties of fly ash and slag blended geopolymer concrete cured at ambient temperature, New Dev. Struct. Eng. Constr. S. Yazdani, A. Singh, (Eds.) ISEC-7, Honolulu, June 18-23, 2013.
[38] X.N. Irani, G. Suresh, P. Rampanth, Experimental studies of ambient cured geopolymer concrete, IOSR J. Mech. Civ. Eng. 14 (3) (2017) 44–49.
[39] N.K. Lee, H.K. Lee, Setting and mechanical properties of alkali-activated fly ash/slag concrete manufactured at room temperature, Constr. Build. Mater. 47 (2013) 1201–1209.
[40] M.N.S. Hadi, N.A. Farhan, M.N. Sheikh, Design of geopolymer concrete with GGBFS at ambient curing condition using the Taguchi method, Constr. Build. Mater. 140 (2017) 424–431.
[41] P. Nath, P.K. Sarker, Effect of GGBFS on setting, workability and early strength properties of fly ash geopolymer concrete cured in ambient condition, Constr. Build. Mater. 66 (2014) 163–171.
[42] Nigerian Industrial Standard (NIS) 441-1, Composition, Specifications and Conformity Criteria for Common Cements. NIS, Lagos, Nigeria, 2003.
[43] British Standard EN 197-1, Cement: Composition, Specifications and Conformity Criteria for Common Cements, BSI, London, 2016.
[44] Nigerian Industrial Standard 441-1, Industrial Standard Order for Cement Manufacturing, Distribution, Classification, and Usage. NIS, Lagos, Nigeria, 2014.
[45] Standards Organization of Nigeria, Standards Organization of Nigeria's Newsletter. Industrial Standard Order for Cement in Nigeria, Lagos, Nigeria, 2014.
[46] British Standard EN 196- 3, Method of Testing Cement: Physical Test, BSI, London, 2016.
[47] British Standard EN 196-6, Methods of Testing Cement: Determination of Fineness, BSI, London, 2018.
[48] British Standard EN 15167-1, Ground Granulated Blast Furnace Slag for Use in Concrete, Mortar and Grout: Definitions, Specifications, and Conformity Criteria, BSI, London, 2006.
[49] A.M. Neville, Properties of Concrete, fifth ed., Pearson Education Ltd., England, 2011.
[50] P. Suwanmaneechot, T. Nochaiya, P. Julphunthong, Improvement, characterization, and use of waste corn cob ash in cement-based materials, IOP Conf. Series: Mater. Sci. Eng. 103 (2015), https://doi.org/10.1088/1757-899X/103/1/012023 012023.
[51] British Standard EN 12620, Aggregates from Natural Sources for Concrete, BSI, London, 2013.
[52] N.P. Rajamane, R. Jeyalakshmi, Quantities of Sodium Hydroxide Solids and Water to Prepare Sodium Hydroxide Solution of Given Molarity for Geopolymer Concrete Mixes, Indian Concrete Institute Technical Paper, SRM University, India, 2014.
[53] British Standard 1008, Mixing water for concrete: Specification for Sampling, Testing, and Assessing the Suitability of Water. BSI, London, 2002.
[54] British Standard EN 206, Concrete Specifications, Performance, Production and Conformity. BSI, London, 2016.
[55] D. Abdul-Manan, Exploring the potential of alternative pozzolana cement for the northern savannah ecological zone in Ghana, American J. Civ. Eng. 4 (30) (2016) 74–79.
[56] K.D. Oluborode, I.O. Olofintuyi, Strength evaluation of corn cob ash in a blended Portland cement, Int. J. Eng. Inno. Technol. 4 (12) (2015) 14–17.
[57] A. Price, R. Yeargin, E. Fini, T. Abu-Lebdeh, Investigating effects of the introduction of corncob ash into Portland cements concrete: Mechanical and thermal Properties, American J. Eng. Appl. Sci. 7 (2014) 133–144.
[58] British Standard 1881-125, Testing Concrete: Methods for Mixing and Sampling Fresh Concrete in the Laboratory, BSI, London, 2013.
[59] British Standard EN 12390-2, Testing Hardened Concrete: Making and Curing for Strength Tests, BSI, London, 2019.
[60] British Standard EN 12350-2. Testing Fresh Concrete: Method for Determination of Slump, BSI, London, 2009.
[61] British Standard EN 12350-4. Testing Fresh Concrete: Method for Determination of Compacting Factor, BSI, London, 2009.
[62] British Standard EN 12390- 4, Testing Hardened Concrete: Compressive Strength of Test Specimens, BSI, London, 2019.
[63] British Standard EN 12390 -5, Testing Hardened Concrete: Flexural Strength of Test Specimens, BSI, London, 2019.
[64] British Standard EN 12390-6, Testing Hardened Concrete: Splitting Tensile Strength of Test Specimens, BSI, London, 2019.
[65] Australian Standards 3600, Concrete Structures. Standards Australia International Ltd, Sydney, NSW, 2019.
[66] K. Neupane, Fly ash and ground granulated blast furnace slag based powder-activated geopolymer binders: A viable sustainable alternative to Portland cement in the concrete industry, Mech. Mater. 103 (2016) 110–122.
[67] British Standard EN 1992-1-1, Design of Concrete Structures: General Rules for Structural Fire Design, BSI, London, 2014.
[68] M. Sofi, J.S.J. Deventer, P.A. Mendis, G.C. Luckey, Engineering properties of geopolymer concrete, Cem. Concr. Res. 37 (2007) 364–369.
[69] B. Tempest, Engineering Characterization of Waste-derived Geopolymer Cement Concrete for Structural Applications, Retrieved from https//:ibres.uncg.edu/ir/uncc/f/Tempest_uncc_0694D_10121.pdf.
[70] G. Lavanya, J. Jegan, Evaluation of the relationship between split tensile strength and compressive strength for geopolymer concrete of varying grades and molarity, Int. J. Applied Eng. Res. 10 (15) (2015) 35523–35527.
[71] E.I. Diaz, E.N. Allouche, S. Vaidya, Mechanical properties of fly ash-based geopolymer concrete, ACI Mater. J. 108 (3) (2011) 300–306.
[72] British Standard EN 450-1, Pozzolan for Use in Concrete: Definitions, Specifications, and Conformity Criteria, BSI, London, 2012.
[73] British Standard EN 8615-2, Specification for Pozzolanic Materials for use with Portland Cement: High Reactivity Natural Calcined Pozzolana, BSI, London, 2019.
[74] N.M. Al Akhras, Durability of metakaolin concrete to sulfate attack, Cem. Concr. Res. 36 (9) (2006) 1727–1734.
[75] D.A. Adesanya, A.A. Raheem, A study of the workability and compressive strength characteristics of corn cob ash blended cement concrete, Constr. Build. Mater. 23 (2009) 311–317.
[76] D.A. Adesanya, A.A. Raheem, Development of corn cob ash blended cement, Constr. Build. Mater. 23 (2009) 347–352.
[77] D.A. Adesanya, A.A. Raheem, A study of the permeability and acid attack of corn cob ash blended cement, Constr. Build. Mater. 24 (2010) 403–409.
[78] M. Behim, M. Beddar, P. Clastres, Reactivity of granulated blast furnace slag, Slovak J. Civ. Eng. 21 (2) (2013) 7–14.
[79] T. Xie, P. Visintin, A unified approach for mix design of concrete containing supplementary cementitious materials based on reactivity moduli, J. Clean. Prod. 203 (2018) 68–82.
[80] British Standard EN 196-2, Methods of Testing Cement: Chemical Analysis of Cement, BSI, London, 2016.
[81] X. Wan, D. Hou, T. Zhao, L. Wang, Insights on molecular structure and micro properties of alkali-activated slag materials: a reactive molecular dynamics study, Constr. Build. Mater. 139 (2017) 430–437.
[82] J. Wongpa, K. Kiattikomol, C. Jaturapitakkul, P. Chindaprasirt, Compressive strength, modulus of elasticity, and water permeability of inorganic polymer concrete, Mater. Des. 31 (10) (2010) 4748–4754.
[83] J. Temuujin, R.P. Williams, A. Van Riessen, Effect of mechanical activation of fly ash on the properties of geopolymer cured at ambient temperature, J. Mater. Process. Technol. 209 (12) (2009) 5276–5280.
[84] A. Nazari, S. Riahi, SiO2 nanoparticles' effects on properties of concrete using ground granulated blast furnace slag as a binder, Mag. Conc. Res. 64 (4) (2012) 295–306.
[85] Concrete Institute of Australia, Geopolymer Concrete: Recommended Practice, CIA, North Sydney, 2016.
[86] British Standard 8500-1, Concrete: Method of Specifying and Guidance for the Specifier, BSI, London, 2015.
[87] D.B. Raijiwala, H.S. Patil, Geopolymer concrete: a concrete of next decade, J. Eng. Res., Stud. 2 (1) (2011) 129–138.
[88] M. Olivia, H. Nikraz, Properties of fly ash geopolymer concrete designed by Taguchi method, Mater. Des. 36 (2012) 191–198.
[89] I. Garcia-Lodeiro, A. Palomo, A. Fernández-Jiménez, D.E. Macphee, Compatibility studies between N-A–S–H and C–A–S–H gels. Study in the ternary diagram Na_2O-CaO-Al_2O_3-SiO_2–H_2O, Cem. Concr. Res. 41 (9) (2011) 923–931.
[90] K.H. Yang, J. Song, K.S. Lee, A.F. Ashour, Flow and compressive strength of alkali-activated mortars, ACI. Mater. J. 106 (1) (2009) 50–58.
[91] K.S. Anil, P.V. Sivapullaiah, Ground granulated blast furnace slag amended fly ash as an expansive soil stabilizer, Soil Found. 56 (2) (2016) 205–212.
[92] S. Diamond, The microstructure of cement paste and concrete - a visual primer, Cem. Concr. Compos. 26 (8) (2004) 919–933.
[93] J.D. Bapat, Mineral Admixtures in Cement and Concrete, first ed., CRC Press, Boca Raton, 2012.
[94] D. King, The effect of silica fume on the properties of concrete as defined in concrete society report 74, cementitious materials (pp. 29-31), Proc. of the 37th Conf.on Our World in Concr. Struc. Singapore, 2012.
[95] H. Xu, J.V. Deventer, The polymerization of alumino-silicate minerals, Int. J. Min. Pro. 59 (3) (2000) 247–266.
[96] S. Alehyen, M.E.L. Achouri, M. Taibi, Characterization, microstructure, and properties of fly ash-based geopolymer, J. Mater. Environ. Sci. 8 (5) (2017) 1783–1796.
[97] S. Bashir, Effect of alkali materials on geo polymer concrete, Int. J. Civ. Eng. Technol. 6 (1) (2015) 1–13.
[98] K.L. Jain, effect on strength properties of concrete of by using GGBS by partial replacing cement and addition of GGBS without replacing cement, SSRG Int. J. Civ. Eng. 3 (5) (2016) 144–149.
[99] K. Vijai, R. Kumutha, B.G. Vishnuram, Feasibility study on effective utilization of fly ash from two thermal power stations on the development of geopolymer concrete, J. Ind. Pollut. Contr. 28 (1) (2012) 35–40.
[100] P. Nath, P.K. Sarker, Flexural strength and elastic modulus of ambient-cured blended low-calcium fly ash geopolymer concrete, Constr. Build. Mater. 130 (2017) 22–31.